Jouines *et al. Breast Cancer Research* (2025) 27:202
https://doi.org/10.1186/s13058-025-02163-x

Breast Cancer Research

RESEARCH Open Access

Fibrillarin-mediated ribosomal RNA maturation is a novel therapeutic vulnerability in triple-negative breast cancer

Camille Jouines[1†], Piero Lo Monaco[1†], Angéline Gaucherot[1†], Julie Radermecker[1], Caroline Isaac[1], Fleur Bourdelais[1], Marie-Ambre Monet[1], Marion Meyer[1], Mounira Chalabi-Dchar[1], Flora Nguyen Van Long[1], Laury Baillon[1], Carine Froment[2,3], Julien Marcoux[2,3], Christophe Vanbelle[4], Tanguy Fenouil[1], Sébastien Durand[1], Stéphane Giraud[5], Jean-Jacques Diaz[1], Virginie Marcel[1] and Frédéric Catez[1*]

Abstract

Background Triple-negative breast cancer (TNBC) remains one of the most challenging breast cancer subtypes to treat due to the lack of effective therapeutic options. Ribosome biogenesis has recently emerged as a promising therapeutic target across various cancers. Despite the current targeting of ribosome biogenesis through RNA polymerase I (RNA Pol I) inhibition, we speculated that other factors essential for ribosome assembly, such as ribosomal RNA (rRNA) maturation factors, may also represent therapeutic targets in TNBC.

Methods Ribosome biogenesis was evaluated in each breast cancer subtype using expression level of ribosome biogenesis factors from the UCSC XENA database. The sensitivity of TNBC cell to inhibition of ribosome biogenesis was evaluated on the TNBC cell lines MDA-MB-231 and BT-20, either using RNA Pol I inhibitors CX-5461 or BMH-21 or by knocking-down Fibrillarin (*FBL*) gene using an shRNA approach. Tumor cell growth and survival was monitored both in vitro and as xenografted tumors.

Results We demonstrate that ribosome biogenesis-related genes are significantly overexpressed in TNBC compared to other breast cancer subtypes, highlighting its potential role in TNBC progression. Accordingly, we show that RNA Pol I inhibition exerts potent anti-proliferative effects in pre-clinical models of TNBC, both in vitro and in vivo. However, the DNA-damaging activity of RNA Pol I inhibitors raises safety concerns, highlighting the need for alternative strategies to inhibit ribosome biogenesis. To this end, we show that targeting a downstream rRNA maturation step, specifically pre-rRNA cleavage, by inhibiting the maturation factor Fibrillarin, also inhibits tumor growth in TNBC models. Notably, ribosome biogenesis inhibition, through either RNA Pol I or Fibrillarin targeting, induces cell cycle arrest without triggering significant cell death.

†Camille Jouines, Piero Lo Monaco, Angéline Gaucherot have contributed equally.

*Correspondence:
Frédéric Catez
frederic.catez@lyon.unicancer.fr

Full list of author information is available at the end of the article

© The Author(s) 2025. **Open Access** This article is licensed under a Creative Commons Attribution 4.0 International License, which permits use, sharing, adaptation, distribution and reproduction in any medium or format, as long as you give appropriate credit to the original author(s) and the source, provide a link to the Creative Commons licence, and indicate if changes were made. The images or other third party material in this article are included in the article's Creative Commons licence, unless indicated otherwise in a credit line to the material. If material is not included in the article's Creative Commons licence and your intended use is not permitted by statutory regulation or exceeds the permitted use, you will need to obtain permission directly from the copyright holder. To view a copy of this licence, visit http://creativecommons.org/licenses/by/4.0/.

Conclusion These findings establish ribosome biogenesis as a therapeutic vulnerability in TNBC and identify rRNA maturation, and Fibrillarin in particular, as novel targets for potential therapeutic intervention.

Keywords Ribosome biogenesis, rRNA maturation, Fibrillarin, Breast cancer, Therapeutic target

Introduction

Triple-negative breast cancer (TNBC), characterized by the absence of oestrogen and progesterone receptor expression, and of *HER2* gene amplification, accounts for 15–20% of breast cancer cases and represents a challenge in patient care. In particular, hormone therapies or HER2-targeted therapies are ineffective against TNBC, for which the standard-of-care remains neoadjuvant/pre-operative chemotherapy followed by surgery and post-surgical treatments [1]. The efficacy of these treatments is limited, and relapses are common due to the metastatic nature of TNBC. Patients harbouring TNBC have a 5-year survival rate ranging from 20 to 50%, depending on the metastatic site, highlighting the inter-tumor heterogeneity of TNBC [2]. New therapies are available or under clinical evaluation, such as immunotherapy, PARP inhibitors, and the antibody–drug conjugate sacituzumab govitecan. However, response rates to these therapies remain below 30%, and adverse effects have been described [1, 3].

New cancer therapeutic prospects have recently emerged from targeting ribosome biogenesis. Indeed, overactivation of ribosome biogenesis is a hallmark of cancer cells, that is typically driven by the dysregulation of signalling pathways that control RNA Pol I activity, such as mTOR and c-MYC, p53 and PTEN [4]. Importantly, tumor cells rely on the overactivation of ribosome biogenesis, which leads to an increase in the number of ribosomes, thus accelerating protein synthesis and metabolism, and favouring cell plasticity and adaptation to various stresses and changes in their environment, including chemotherapy [5]. Ribosome biogenesis inhibition triggers ribosomal stress, which leads to a cytotoxic response that may include apoptosis, cell cycle arrest and autophagy depending on the cell type [6]. Recently developed RNA Pol I inhibitors CX-5461 and BMH-21 provided the proof-of-concept that inhibiting ribosome biogenesis reduces cancer cell activity [7, 8]. CX-5461 and BMH-21 inhibits RNA Pol I by binding to G-quadruplex and GC-rich DNA sequences respectively, which are both abundant within the rDNA loci[7, 8]. However, off-target effects, specifically DNA damage, have been reported for CX-5461, likely due to DNA replication defects [9]. Their therapeutic potential has so far been explored in various solid and haematological cancers, including leukaemia, lymphoma, myeloma, osteosarcoma, prostate cancer, ovarian cancer, glioma and neuroblastoma, but not in triple negative breast cancer [7, 8, 10–12]. This dependency on ribosome biogenesis and its factors thus represents a vulnerability for cancer cells, which could be exploited as a therapeutic approach [5, 13].

Though targeting RNA Pol I activity is the main strategy used to inhibit ribosome biogenesis, other factors could constitute promising candidates. Indeed, human ribosomes are assembled through a highly complex sequential and regulated process, that includes pre-ribosomal RNA (rRNA) endonuclease and exonuclease cleavages to release the mature 18S, 5.8S and 28S rRNAs, chemical modifications, folding and assembly with the 80 ribosomal proteins. These processes rely on hundreds of chaperones, nucleases, RNA helicases and non-coding C/D box and H/ACA small nucleolar RNAs (snoRNAs). Importantly, many of these ribosome biogenesis factors are essential to ribosome maturation, and may therefore be considered as therapeutic targets [13, 14]. For instance, inhibiting the non-coding U3 and U8 C/D box snoRNAs prevents the processing of pre-rRNAs into mature 18S and 28S rRNAs, and has anti-tumoral effects both in vitro and in vivo [15]. Similarly, the Fibrillarin (FBL) protein, a key component of the C/D box snoRNP complexes, is also required for proper ribosome production in yeast and human cells [14, 16–19]. FBL contributes to mammary tumorigenesis and is overexpressed in several cancers, including breast cancer [17, 20], acute myeloid leukaemia [21], prostate [22] and liver cancers [23]. In addition, in breast cancer, high FBL expression levels are associated with a poor prognosis [20].

Here, using pre-clinical in vitro and in vivo models, we demonstrate that ribosome biogenesis is a therapeutic vulnerability in TNBC, by inhibiting RNA Pol I activity and FBL-mediated rRNA maturation steps. We conclude that targeting rRNA maturation may offer a safer therapeutic strategy by avoiding the use of DNA binding compounds.

Results

The level of ribosome biogenesis-associated genes is higher in TNBC compared to other breast cancer subtypes

The molecular characterization of breast cancer subtypes has been instrumental in understanding their biology and identifying vulnerabilities for therapeutic intervention. As for other cancers, increased ribosome biogenesis is a hallmark of breast cancer cells [17, 20, 24], albeit it is unclear whether different levels of ribosome biogenesis are associated with specific breast cancer subtypes. To address this, we studied the level of expression of ribosome biogenesis-associated genes, used as a surrogate of ribosome biogenesis overactivation, as previously

reported [20]. We compared their levels across the different breast cancer subtypes using the BRCA gene expression dataset from The Cancer Genome Atlas (TCGA) public database [25]. The ribosome biogenesis-associated gene signature encompassed 240 genes that defined the KEGG pathway "Ribosome Biogenesis in Eukaryotes" (Supplementary Table S1). Tumor samples (n = 739) were first categorized into four breast cancer subtypes based on the PAM50 molecular classification (Supplementary Table S2 and S3). The expression levels of ribosome biogenesis-associated genes were significantly higher in TNBC than in all other molecular breast cancer subtypes, including luminal A, luminal B and HER2-enriched (ANOVA, $p = 2.79 \times 10^{-53}$; Fig. 1A). This finding was confirmed in a second group of tumor samples (n = 712) categorized according to their histological classification (*i.e.*, intrinsic breast cancer subtype) (ANOVA, $p = 3.82 \times 10^{-29}$; Fig. 1B). Of note, despite using distinct parameters (histological and molecular) the groups of the two classifications overlapped (Supplementary Table S3). These results suggest that ribosome biogenesis is more active in TNBC than in other breast cancer subtypes.

CX-5461 and BMH-21 display on- and off-target activities in TNBC cells

Given that ribosome biogenesis is overactivated in TNBC, we investigated the impact of its inhibition on TNBC cell lines by blocking RNA Pol I activity, using CX-5461 and BMH-21, two of the most extensively studied RNA Pol I inhibitors. We first determined whether CX-5461 and BMH-21 inhibited RNA Pol I activity in TNBC cells. rRNA synthesis was evaluated by RNA FISH performed using two probes binding to the 5'-ETS and ITS1 regions of the pre-rRNA for the detection of both long- and short-lived pre-rRNA intermediates. In the TNBC cell lines MDA-MB-231 and BT-20, both CX-5461 and BMH-21 efficiently inhibited pre-rRNA synthesis after 4 h of treatment at 1 µM (Fig. 2A). Single cell measurement of the RNA FISH signal revealed that BMH-21 was as effective as actinomycin D, used as reference inhibitor of RNA Pol I to inhibit rRNA synthesis, unlike CX-5461 for which inhibition was not complete, as previously described (Figure S1) [7]. Furthermore, consistent with its mechanism of action [8], BMH-21 treatment resulted in the destabilization of the RPA-194 RNA Pol I subunit, which decreased by 30% in MDA-MB-231 and 65% in BT-20 cells (Fig. 2B). We observed that CX-5461 also reduced RPA-194 by 50% in BT-20, but not in MDA-MB-231, an effect not previously reported (Fig. 2B). These data confirmed the high level of activity of CX-5461 and BMH-21 towards RNA Pol I in TNBC cells.

Previous studies have reported conflicting data on possible off-target activity of CX-5461 and BMH-21, especially DNA damage induction, due to their mode of action, binding respectively to G-quadruplex and GC-rich DNA sequences. While DNA damage by BMH-21 remains uncertain, several reports clearly described a genotoxic effect of CX-5461 in some pre-clinical models, likely due to a topoisomerase II inhibitor activity [9, 26]. Here, DNA damage induction was monitored in TNBC cells by γ-H2AX staining 24 h after treatment with 1 µM of CX-5461 and BMH-21 (Fig. 2C and 2D). The level of γ-H2AX staining and the number of its foci, increased

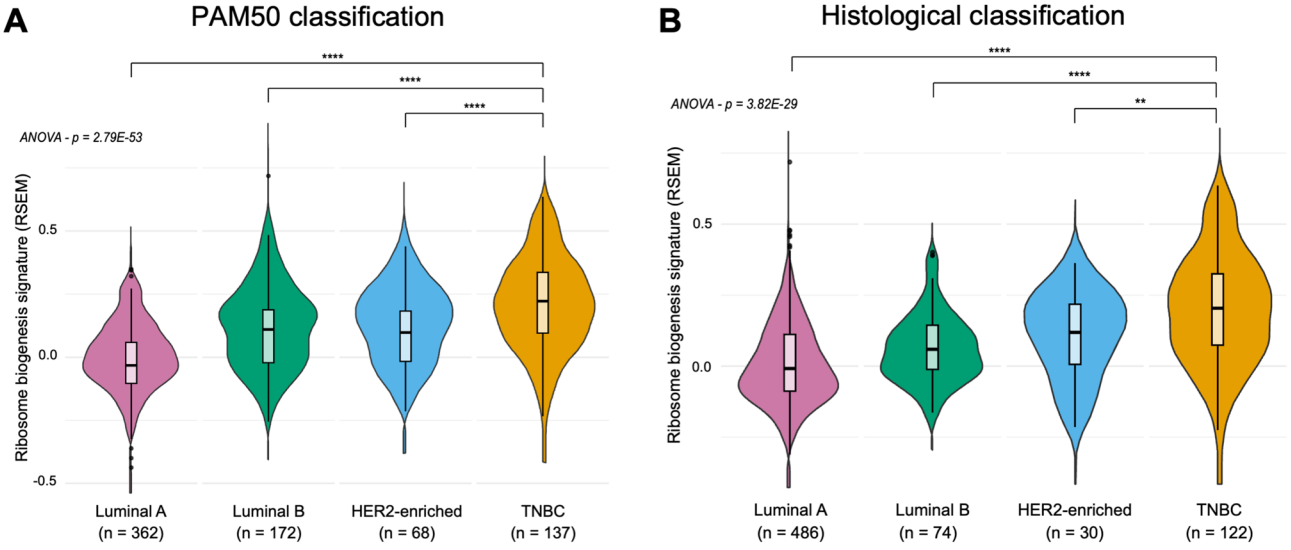


Fig. 1 Ribosome biogenesis is higher in TNBC tumors. Comparison of the median expression of ribosome biogenesis genes (240 genes, see Supplementary Table S1) between the different breast cancer subtypes extracted from the UCSC XENA database. The different breast cancer subtypes were defined using either the PAM50 (**A**) or the histological (**B**) classification. n: number of samples; ** $p < 0.01$, *** $p < 0.001$ **** $p < 0.0001$ (ANOVA test, Student test, Mann–Whitney test)

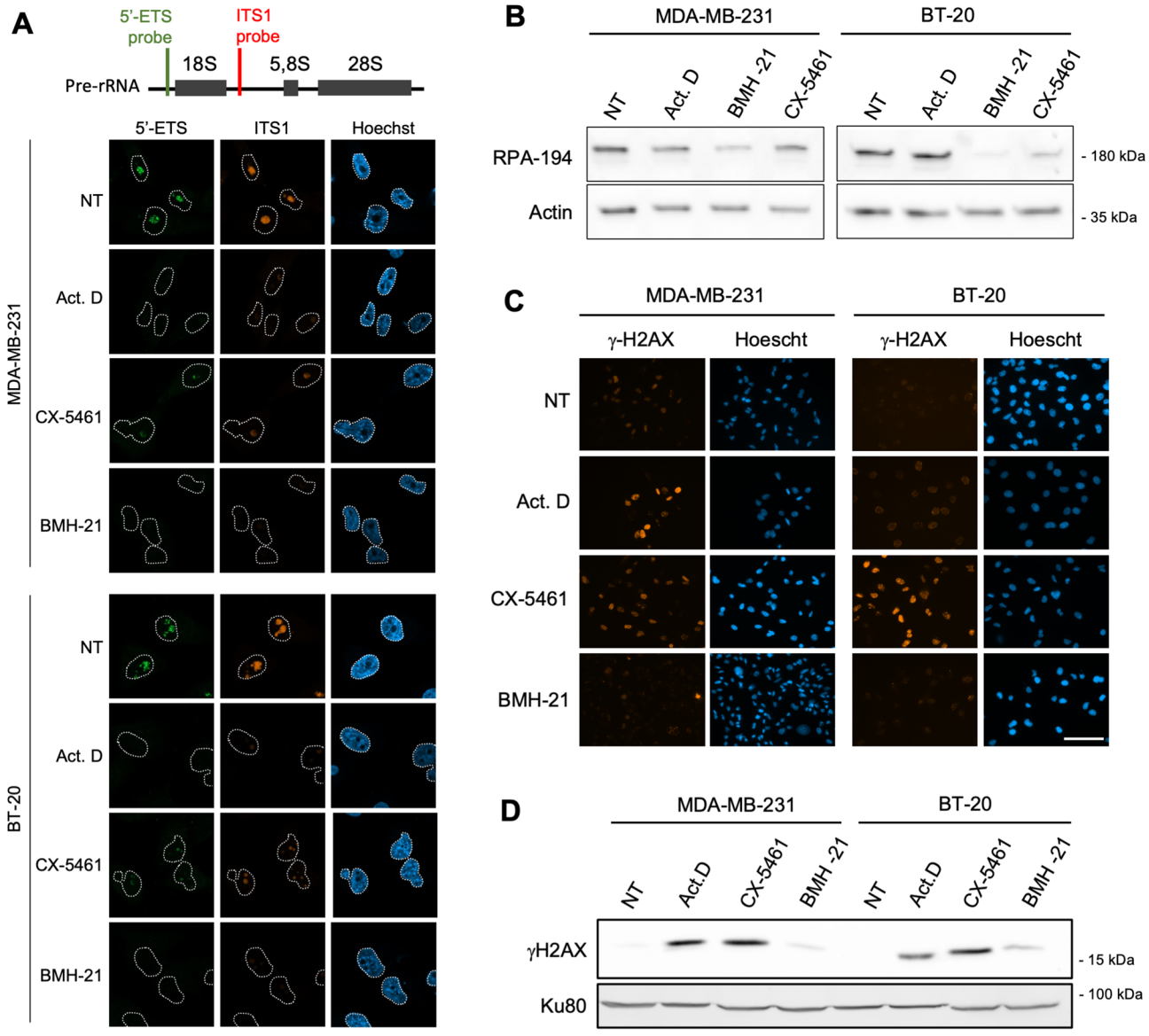


Fig. 2 CX-5461 and BMH-21 inhibit RNA Pol I and induce DNA damage in TNBC cells. **A,** Representative images of FISH detection of the pre-rRNA using probes specific to 5'-ETS and ITS1 region in MDA-MB-231 and BT-20 cells, either untreated (NT) or treated with 1 µM CX-5461, 1 µM BMH-21, or 0.05 µg/mL actinomycin D for 4 h. Nuclei were stained with Hoechst. Scale bar: 20 µM. **B,** Immunoblot of RPA-194 protein in MDA-MB-231 and BT-20 cell lines either untreated (NT) or treated with 1 µM CX-5461, 1 µM BMH-21, or 0.05 µg/mL actinomycin D for 4 h. Data representative of 2 independent biological replicates. **C,** Immunofluorescence staining of γ-H2Ax in MDA-MB-231 and BT-20 cells either untreated (NT) or treated with 1 µM CX-5461, 1 µM BMH-21, or 0.05 µg/mL actinomycin D for 24 h. Nuclei were stained with Hoechst. Scale bar: 50 µM. Images are representative of 3 independent biological replicates. **D,** Immunoblot of γ-H2Ax levels in MDA-MB-231 and BT-20 cells lines either untreated (NT) or treated with 1 µM CX-5461, 1 µM BMH-21, or 0.05 µg/mL actinomycin D for 24 h. Data representative of 2 independent biological replicates

after CX-5461 and actinomycin D treatment, but not after exposure to BMH-21 (Fig. 2C), a result confirmed by Western blot (Fig. 2D). Hence, the RNA Pol I inhibitor CX-5461 induces DNA damage in TNBC cells in vitro, while BMH-21 has a very limited impact. Overall, these results demonstrate that RNA Pol I inhibitors CX-5461 and BMH-21 can effectively inhibit ribosome biogenesis in TNBC cells, and that CX-5461 also displays an off-target activity owing to its genotoxic effect, and are consistent with previously published data on cell lines from other cancers [9, 26].

CX-5461 and BMH-21 reduce TNBC cell growth in vitro

To evaluate the antitumor activity of the RNA Pol I inhibitors on TNBC cells, the MDA-MB-231 and BT-20 cell lines were treated with CX-5461 and BMH-21 at concentrations ranging from 1–1,000 nM. Both compounds exhibited dose-dependent activities on TNBC

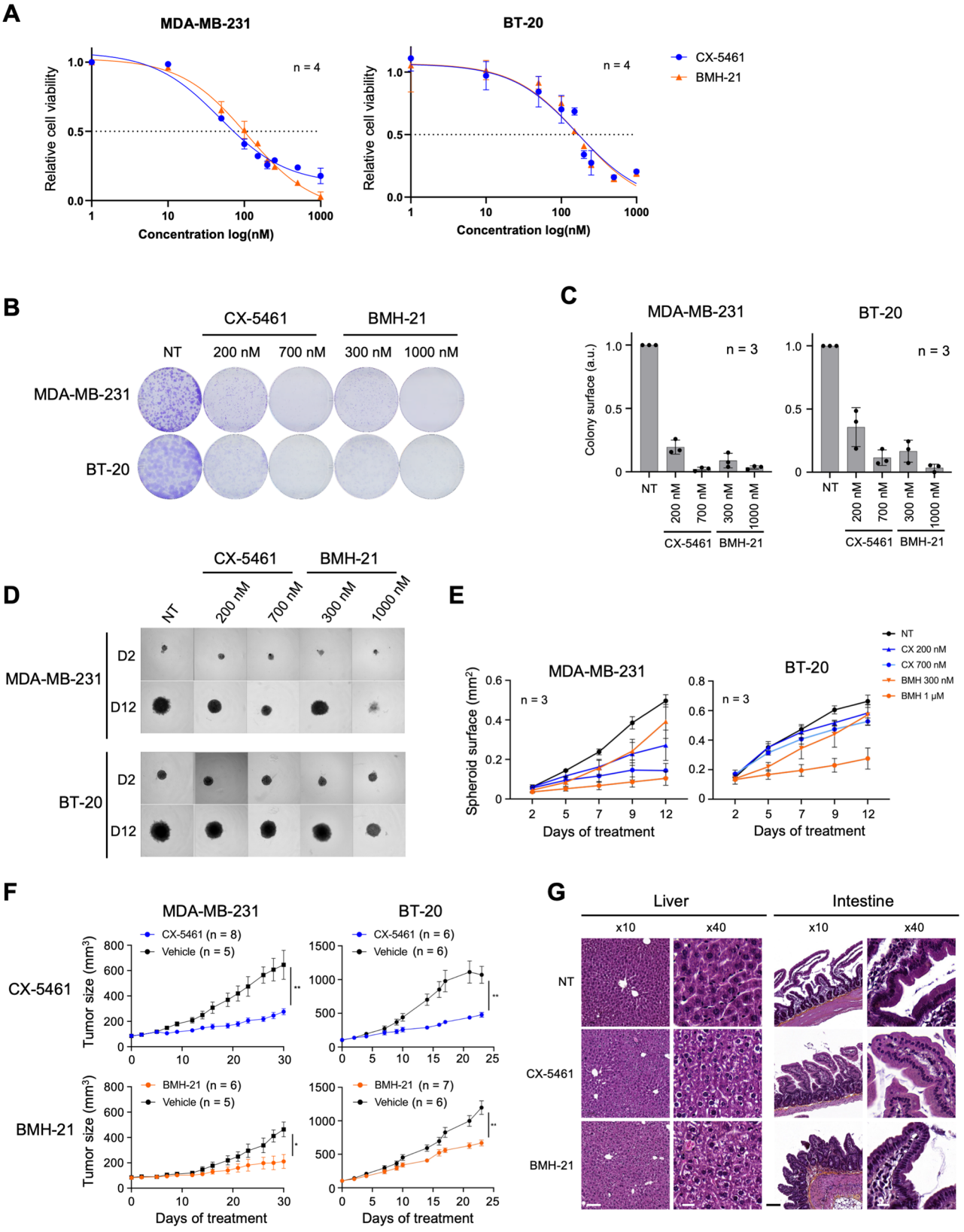


Fig. 3 (See legend on next page.)

(See figure on previous page.)

Fig. 3 Inhibition of RNA Pol I reduces tumorigenesis in vitro and in vitro in TNBC. **A,** Relative cell proliferation of MDA-MB-231 and BT-20 cells following treatment with 1–1,000 nM CX-5461 and BMH-21. Error bars correspond to the s.d. of 4 biological replicates. **B-C,** Colony formation assay on MDA-MB-231 and BT-20 cells, either untreated (NT) or treated with CX-5461 or BMH-21, at the indicated concentration for 10 days. The surface of the colony was quantified (**C**) from the images in (**B**). The result is representative of 3 independent biological replicates. The data are presented as mean ± s.d. **D,** Spheroid growth of MDA-MB-231 and BT-20 cells either untreated (NT) or treated with CX-5461 or BMH-21 at the indicated concentrations. Images shown were collected 2- or 12-days post-treatment. **E,** the size of the spheroids was quantified from the images in (**D**). The results are mean ± SEM from 3 technical replicates, and are representative of 3 biological replicates. **F,** Growth of tumor xenografts of MDA-MB-231 and BT-20 cells over 30 days, in mice treated with CX-5461 or BMH-21 at 50 mg/kg, or vehicle at day 0. Quantification of tumor volume is presented as mean ± SEM (n = 5). * $p < 0.05$, ** $p < 0.01$ (Student t-test) **G,** Hematoxyline-eosine staining of liver and intestine tissue sections, from mice treated 23 days with CX-5461 or BMH-21 or from control animals (Vehicle). Images were collected using a × 10 and × 40 objective. Scale: at × 10 = 100 µm; at × 40 = 20 µm. Representative images of 3 animals

cell proliferation (Figs. 3A and S2A). IC_{50} values were calculated for each cell line based on cell confluence after 96 h of treatment. The IC_{50} values for CX-5461 in MDA-MB-231 and BT-20 cells were 49.62 nM and 163.5 nM, respectively. For BMH-21, the IC_{50} values were 107.2 nM in MDA-MB-231 and 172.7 nM in BT-20 (Fig. 3A). Thus, low concentrations of both compounds induced toxicity, with IC_{50} values in the nanomolar range in both cell lines. We then assessed the effects of CX-5461 and BMH-21 on the clonogenic potential of TNBC cells. Treatments with either compound significantly reduced the number of colonies formed by both cell lines compared to untreated controls at all tested concentrations, notably at 200 nM of CX-5461 and 300 nM BMH-21 (Fig. 3B and 3C). Indeed, upon exposure to 200 nM CX-5461, the clone surface area decreased by 60% in BT-20 cells and by 80% in MDA-MB-231 cells, with a 90% reduction observed at 700 nM. BMH-21 also reduced the ability of cells to form clones, with surface areas decreasing by 80–90% at 300 nM, and clone formation becoming negligible at higher concentration (1,000 nM) (Fig. 3C). Overall, the two compounds drastically reduced the proliferative capacity of TNBC cells when cultured as a monolayer.

We next evaluated the effects of CX-5461 and BMH-21 on the ability of TNBC cells to grow in 3D as spheroids. TNBC spheroids were treated as indicated 2 days post-formation and were monitored every 2 to 3 days by microscopic observation, and the surface area of each spheroid was measured (Fig. 3D and 3E). Treated spheroids were smaller compared to untreated controls, with a stronger effect observed at higher concentrations. For both cell lines, spheroid growth displayed a reduction as early as day 5 post-treatment in a dose-dependent manner. Exposure to 200 nM or 700 nM CX-5461 for 12 days resulted in a 1.8-fold and 3.4-fold reduction in the size of MDA-MB-231 spheroids, respectively, while only a slight decrease was observed for BT-20 spheroids (Fig. 3D and 3E). Conversely, BMH-21 similarly impacted the growth of spheroids of both cell lines, with a limited impact at 300 nM, and a fivefold reduction on MDA-MB-231 spheroids and 2.4-fold reduction on BT-20 spheroids at 1,000 nM, by day 12 (Fig. 3D and 3E). Overall, our results show that RNA Pol I inhibitors CX-5461 and BMH-21 reduce TNBC cell growth in vitro, even at nanomolar concentrations.

CX-5461 and BMH-21 reduce tumor growth in human TNBC xenografts

The antitumor activity of CX-5461 and BMH-21 was then investigated in MDA-MB-231 and BT-20 xenograft models, upon subcutaneous injection into athymic nude mice. CX-5461 was administered orally at 50 mg/kg three times a week, while BMH-21 was given intraperitoneally at 50 mg/kg five times a week, as previously described [7, 8]. In these models, CX-5461 treatment significantly reduced tumor growth by 2 to 3-fold compared to the control group (from 645 mm^3 to 276 mm^3 in MDA-MB-231, and from 1070 mm^3 to 477 mm^3 in BT-20) (Fig. 3F), and BMH-21 also significantly reduced tumor size, though to a lesser extent (from 463 mm^3 to 210 mm^3 in MDA-MB-231, and from 1093 mm^3 to 669 mm^3 in BT-20) (Fig. 3F). Given the genotoxic activity of CX-5461 in vitro (Fig. 2C-D), we wondered whether it may have a similar effect in xenografts. Consistent with our observation in cultured cells, CX-5461 treatment, but not BMH-21, induced H2AX phosphorylation in the xenografts (Figure S2B, demonstrating that, as in other cancers [9, 26], both RNA Pol I inhibitors impair TNBC tumor growth in vivo, and that CX-5461 alone exhibits an off-target activity.

Importantly, given that ribosome biogenesis occurs in all cells, it was crucial for us to demonstrate the selective effects of RNA Pol I inhibitors on tumors. As previously described, we observed no impact on the body weight of our xenograft models treated with both compounds (Figure S2C) [7, 8]. To further evaluate their potential toxicity, we performed a histological analysis of several organs, including the brain, heart, lungs, liver, kidneys, pancreas, stomach, intestine, and colon. No major lesions were detected in the tissues of mice treated with BMH-21 or CX-5461. However, some moderate histological alterations were noted. In the intestine, villous atrophy was observed in BMH-21-treated mice, while no changes were detected in the intestines of control or CX-5461-treated mice. Additionally, a diffuse oedema was observed in the colon of both BMH-21- and CX-5461-treated mice compared to controls. In the liver,

hepatocytes with clear cytoplasm were diffusely present in BMH-21-treated mice, whereas this effect was localized to the periportal region in CX-5461-treated mice (Fig. 3G). Overall, these findings suggest minimal acute toxicity of CX-5461 and BMH-21 following short-term treatment in mice. However, they highlight the need for caution regarding potential adverse effects associated with long-term use.

CX-5461 and BMH-21 induce cell cycle arrest but no cell death in vitro and in vivo

Ribosome biogenesis inhibition is known to trigger ribosomal stress, which can lead to cell death and/or cell cycle arrest. We thus explored these two cell responses in MDA-MB-231 and BT-20 cell lines. Surprisingly, following three days of treatment, no evidence of cell death was observed using DRAQ7 staining in cells treated with CX-5461 or BMH-21, while accumulating dead cells was observed upon actinomycin D treatment in both MDA-MB-231 and BT-20 cell lines (Figure S3A). To further support this observation, we examined the classical apoptotic markers cleaved caspase-3 and PARP by western blot (Figure S3B). Following treatment with CX-5461 or BMH-21, no cleavage of PARP or caspase-3 was detected in either cell line (Figure S3B). Additionally, treatment with known apoptosis inducers—actinomycin D, doxorubicin, etoposide, or staurosporine—also failed to trigger cleavage of caspase 3 and PARP in these cells, whereas clear activation was observed in HeLa cells, used as a positive control (Figure S3B). Consistently, in the xenograft tumors, immunohistochemical staining of cleaved caspase 3 indicated that apoptosis was not triggered in response to CX-5461 and BMH-21 treatment (Figure S3C). This indicated that the cleaved caspase-3 and PARP pathways are severely impaired in these TNBC cell lines. Thus, CX-5461 and BMH-21 do not induce cell death in these TNBC cell lines both in vitro and in vivo.

Next, we evaluated the effects of CX-5461 and BMH-21 on cell cycle progression. Treatment with CX-5461 (200 and 700 nM) and BMH-21 (300 and 1,000 nM) for 18 h resulted in distinct alterations in cell cycle progression (Figs. 4A and S3D-S3E). For CX-5461, treatment led to a significant accumulation in the G2/M phase in both MDA-MB-231 and BT-20 cells, with higher concentrations also causing an accumulation in the S phase and a reduction in the G1 phase in MDA-MB-231. CX-5461 treatment thus promotes S-phase defect and G2/M checkpoint arrest. For BMH-21, the effects were cell-dependent, with the induction of a significant accumulation of MDA-MB-231 cells in the G1 phase, along with a decrease in the S phase, indicative of a G1/S checkpoint arrest. In contrast, BT-20 displayed no clear alteration of cell cycle despite the growth defect observed (Figs. 3A, 4A and S3D). We further explored the different effects on the cell cycle status induced by the two RNA Pol I inhibitors, by focusing on the M phase through phosphohistone H3 (Ser10) staining (Figure S3E). Compared to CX-5461, BMH-21 treatment induced a marked decrease in phospho-H3, in particular in BT-20 cells, indicating that BMH-21 prevented mitosis (Figure S3D). To determine the relevance of these observations in in vivo models, we performed a concomitant IHC analysis of proliferation (Ki67 marker) and mitosis status (phospho-H3 staining) in xenografted tumors. We observed no difference in the Ki67 signal in the proliferative area of the tumor, for both cell lines and both treatments (Fig. 4B). In contrast, a decrease in phospho-H3 (Ser10) signal was observed in MDA-MB-231 and BT-20 xenografts upon treatment with CX-5461 (Fig. 4B), supporting the cell-type dependent effects of these RNA Pol I inhibitors on cell cycle arrest in vitro and in vivo.

To better understand the TNBC cell response to these inhibitors, we then performed a label-free quantitative proteomics analysis on whole cell extracts of MDA-MB-231 cells treated with CX-5461, BMH-21 or actinomycin D as a reference treatment. The analysis identified and quantified 4,513 proteins. To evaluate changes in protein levels, pairwise comparisons based on mass spectrometry (MS) peak intensity values were performed for each protein between treated and untreated condition. Each treatment induced a notable alteration in the cell proteome (Figure S4 and Table S6), with significant alterations of the level of 277 proteins in actinomycin D treated cells, 127 proteins in CX-5461 treated cells and 156 proteins in BMH-21 treated cells (Figure S4). Interestingly, among the differentially expressed proteins following BMH-21 and actinomycin D treatment, a majority were down-regulated (76.9% and 81.2 respectively), whereas following CX-5461 treatment a minority of proteins were down-regulated (34.0%), reflecting a different impact on the cell gene expression (Figure S4). We then performed a Gene Ontology (GO) analysis in order to identify the most altered cellular functions (Fig. 4C and supplementary table S7). The most represented GO Terms were very different among the three conditions, actinomycin D and BMH-21 treatments being associated with ribosome biogenesis and nucleic acid-related cellular functions, while CX-5461 treatment was associated with cell division-related cellular functions (Fig. 4C). These findings further characterize BMH-21 as a *bona fide* ribosome biogenesis inhibitor, and support that CX-5461 does not act as a ribosome biogenesis inhibitor but rather as a cell division inhibitor. Collectively, these findings emphasize the potential of ribosome biogenesis as a therapeutic target in TNBC. However, they also highlight the need for developing more specific strategies to inhibit ribosome biogenesis, while minimizing off-target effect.

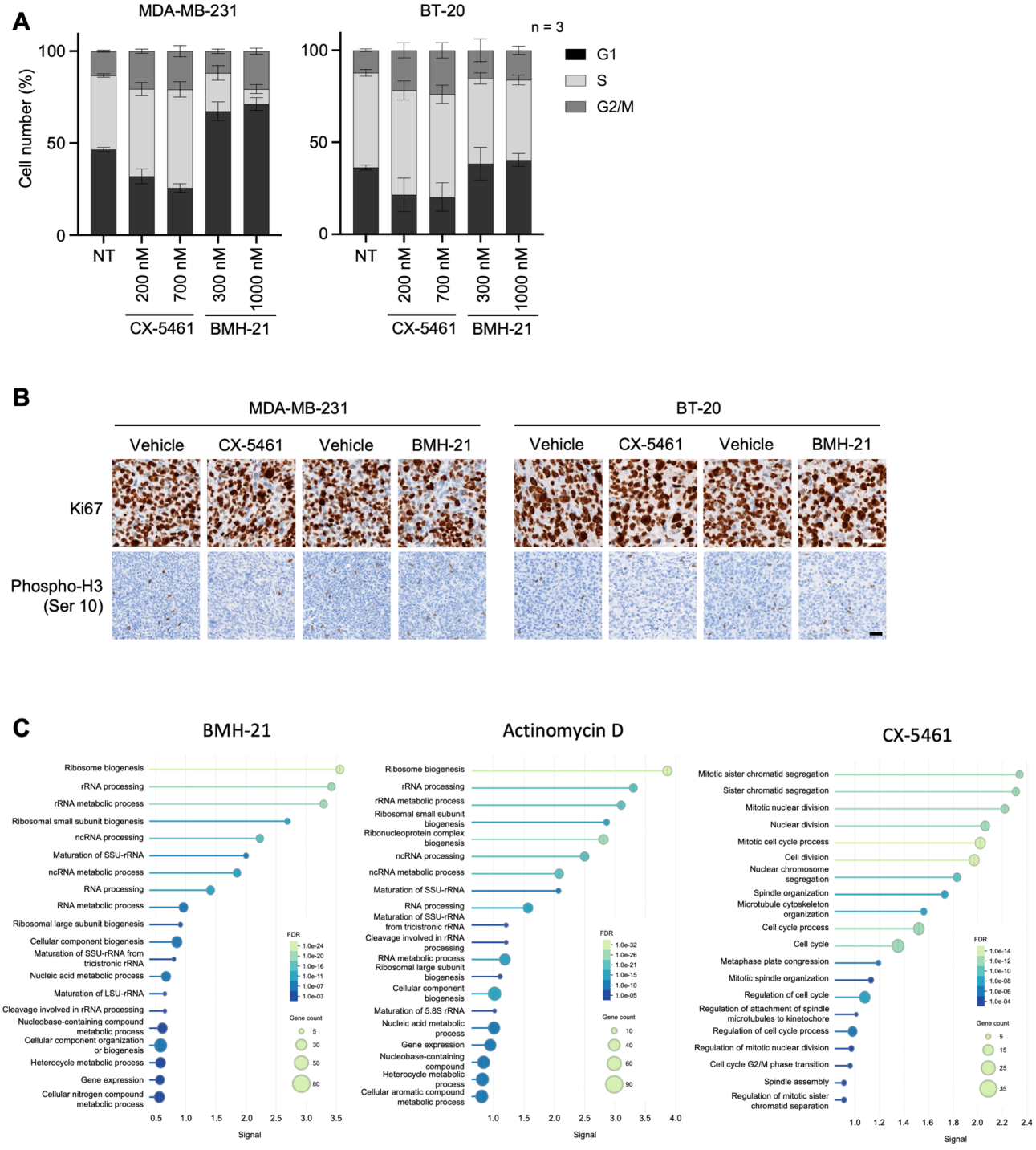


Fig. 4 Impact of CX-5461 and BMH-21 on cell cycle and ribosome biogenesis in TNBC cells in vitro.**A,** Proportion of cells in G1, S, and G2 phases of the cell cycle of MDA-MB-231 and BT-20 cells, either untreated (NT) or treated with CX-5461 or BMH-21, at the indicated concentrations or with actinomycin D at 0.05 µg/mL for 18 h. Error bars correspond to the s.d. from three technical replicates. Results are representative of six biological replicates. **B,** IHC staining of the proliferation marker Ki67 and mitosis marker phospho-Histone H3 (Ser 10), on sections of xenograft tumors, from the experiment shown in Fig. 3F. Images are representative of 5 biological replicates. Scale bar: 50 µm. **C,** Gene ontology analysis performed on proteomic data obtained on whole cell extracts of MDA-MB-231 cells treated with CX-5461, BMH-21 or actinomycin D for 18 h (see Table S6). The graph shows the 20 most represented GO terms (see Table S7) among the differentially expressed genes compared to untreated cells. The data were obtained from 5 biological replicates

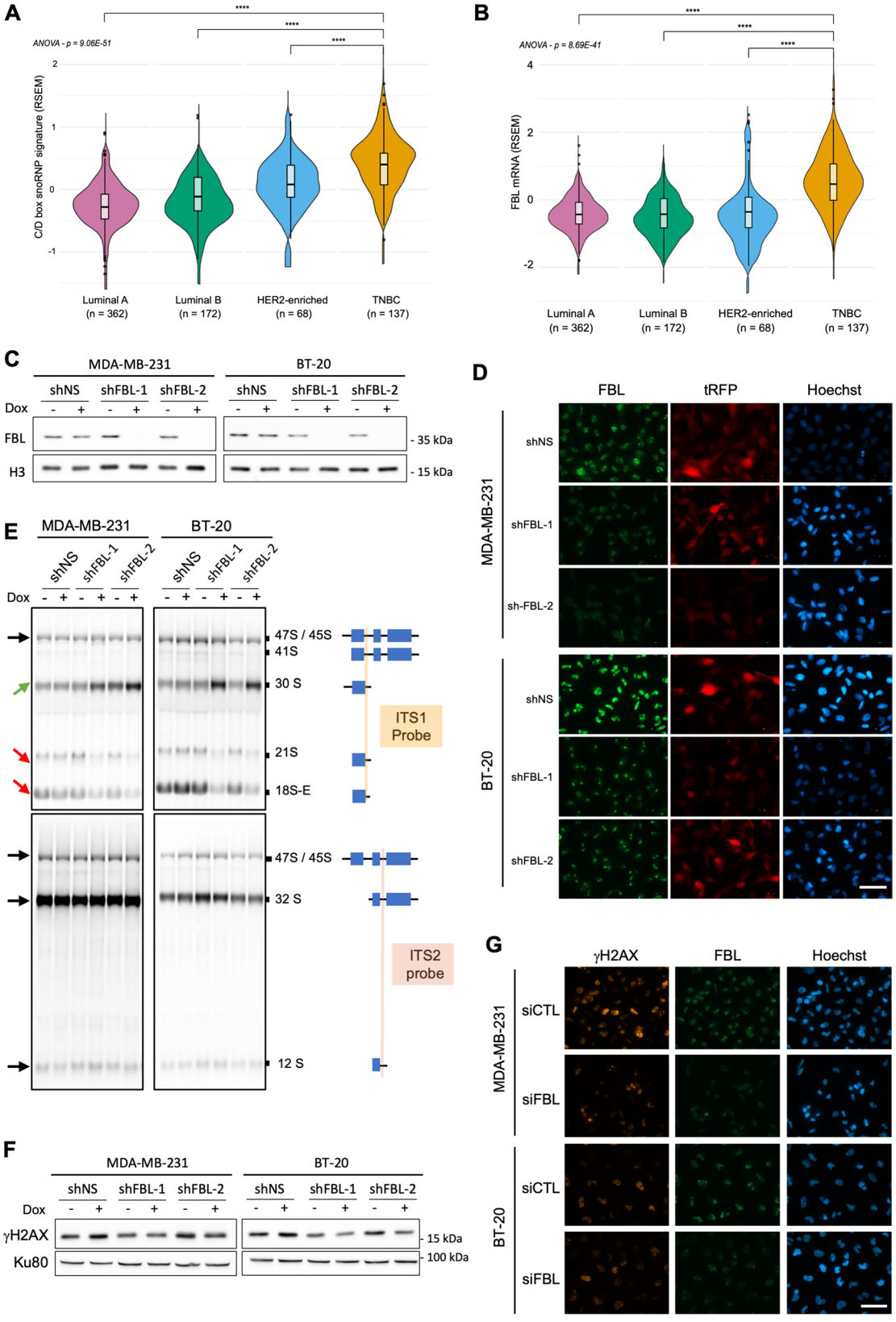


Fig. 5 (See legend on next page.)

(See figure on previous page.)

Fig. 5 FBL knock-down inhibits maturation of pre-rRNA whithout inducing DNA damage. **A-B,** Comparison of the median expression of mRNAs of C/D box snoRNP protein genes (**A**) (FBL, NOP56, NOP58, NHP2L1) or of FBL (**B**), between each breast cancer subtypes. Normalized transcriptomic data were extracted from the UCSC XENA database. The breast cancer subtypes were defined using the PAM50 classification. n: number of patients, **** $p < 0.0001$ (ANOVA test, Mann–Whitney test). **C,** FBL protein levels analysed by Western blot in MDA-MB-231 and BT-20 cell lines after 96-h doxycycline-mediated shRNA induction. The cell lines express either a control non-silencing shRNA (shNS) or a shRNA-targeting FBL (FBL-1 and FBL-2). Data are representative of 3 independent replicates. **D,** Immunofluorescence staining of FBL in MDA-MB-231 and BT-20 cell lines after 96-h doxycycline-mediated shRNA induction (shFBL-1, FBL-2, and shNS). The tRFP protein is co-expressed with the shRNA and is used as a marker of doxycycline induction. The images are representative of 3 biological replicates. Scale bar: 50 µm. **E,** Northern blot analysis of pre-rRNA processing in MDA-MB-231 and BT-20 cells after 96-h doxycycline-mediated shRNA induction (shFBL-1, FBL-2, and shNS). The positions of the probes used and the detected pre-rRNA species are indicated on the right. Arrows on the left show the trends of each pre-rRNA species in shRNA-induced cells relative to non-induced cells. Data representative of two biological replicates. **F,** Western blot analysis of γ-H2Ax protein levels in MDA-MB-231 and BT-20 cell lines after 96-h doxycycline-mediated shRNA induction (shFBL-1, FBL-2, and shNS). Data representative of two biological replicates. **G,** Immunofluorescence staining of γ-H2Ax and FBL in MDA-MB-231 and BT-20 cells transfected with a FBL siRNA or a control siRNA. Scale bar: 50 µm

FBL expression is higher in TNBC compared to other breast cancer subtypes

Having shown that ribosome biogenesis is a druggable vulnerability of TNBC, we next sought to identify other ribosome biogenesis factors that could be inhibited for therapeutic purposes. Once the rRNA precursor is synthesized by RNA Pol I, it undergoes several essential cleavages that release the 18S, 5.8S and 28S [27]. C/D box snoRNP containing the U3 snoRNA is required for a cleavage step within the 5'-ETS that is essential for rRNA maturation. It has been reported that the knock-down of U3 snoRNA decreases the growth of lung and luminal breast cancer cells, and prevents tumor initiation of lung cancer cell xenografts [15]. In addition, we have previously shown that the knock-down of FBL, a central component of the C/D box snoRNP, inhibits the U3 snoRNA-driven cleavage step within the 5'-ETS region of the pre-rRNA [16]. We thus explored FBL as a potential therapeutic vulnerability in TNBC. We previously demonstrated that elevated *FBL* mRNA levels are associated with poor survival in breast cancer patients, although this analysis did not focus on specific breast cancer subtypes [20]. To determine whether the C/D box snoRNP complex signature differs in TNBC, we compared this signature (*i.e.*, FBL, NOP56, NOP58, NHP2L1) in different breast cancer subtypes using the BRCA-TCGA dataset as described above for the ribosome biogenesis signature. The C/D box snoRNP complex signature was significantly higher in TNBC than in other breast cancer subtypes, using either the PAM50 classification (ANOVA, $p = 9.06 \times 10^{-51}$, Fig. 5A) or the histological classification (Figure S5A). Importantly, the expression level of *FBL* itself was higher in the TNBC subtype compared to other breast cancer subtypes (ANOVA, $p = 8.69 \times 10^{-41}$, Fig. 5B and Figure S5B).

FBL knock-down inhibits pre-rRNA maturation and cell growth in vitro without inducing DNA damage in TNBC cells

To assess the impact of FBL knock-down on TNBC cell lines, we established MDA-MB-231 and BT20-based stable cell lines, expressing either two independent FBL shRNAs (*i.e.*, shFBL-1 and shFBL-2) or a negative control shRNA (shNS), in an inducible manner. Effective knock-down of FBL expression was confirmed at the mRNA level by RT-qPCR (Figure S5C) and at the protein level by Western blot (Fig. 5C), showing more than 90% reduction in both mRNA and protein levels. Immunofluorescence imaging revealed a homogeneous decrease in FBL signal within the cell population (Fig. 5D). Of note, we observed a significant reduction in FBL levels from 2 days post-induction onwards in both cell lines (Figure S5D), whereas doxycycline and non-specific shRNA (*i.e.*, shNS) had no impact on its expression. To determine whether FBL knock-down impairs pre-rRNA processing in TNBC cells, Northern blot analysis was performed to examine different cleavage stages of the 18S and 28S/5.8S rRNA processing pathways (Fig. 5E, ITS1 probe and ITS2 probe, respectively). Following 96 h of FBL knockdown, 18S rRNA processing was significantly inhibited, as illustrated by the accumulation of early-stage intermediate species (*i.e.,* 30S pre-rRNA) and a decrease in late intermediate species (*i.e.,* 21S and 18S-E pre-rRNAs). In contrast, no impact on the 28S/5.8S processing pathway was observed (Fig. 5E, ITS2), as previously reported in HeLa cells [16].

Because of the off-target activity observed with the RNA Pol I inhibitors, we wondered whether FBL knock-down induces DNA damage. Our analysis revealed that FBL reduction did not cause detectable DNA damage as assessed by Western blot analysis of γ-H2AX (Fig. 5F) and by immunostaining (Fig. 5G and S5E). These findings were consistent across both shRNA-based (Fig. 5F) and siRNA-based knock-down approaches (Fig. 5G and S5E). Hence, FBL knock-down impairs ribosome biogenesis by blocking the 5'-ETS pre-rRNA maturation, without inducing DNA damage, in our TNBC cellular models.

Given the inhibitory effect of FBL knock-down on TNBC cell ribosome biogenesis, we determined whether its targeting could be anti-tumoral using various in vitro assays. First, we monitored cell growth in real-time. It revealed that FBL knock-down significantly reduced cell proliferation compared to controls (shNS and non-treated cells) (Fig. 6A). Even after 250 h (10 days), FBL

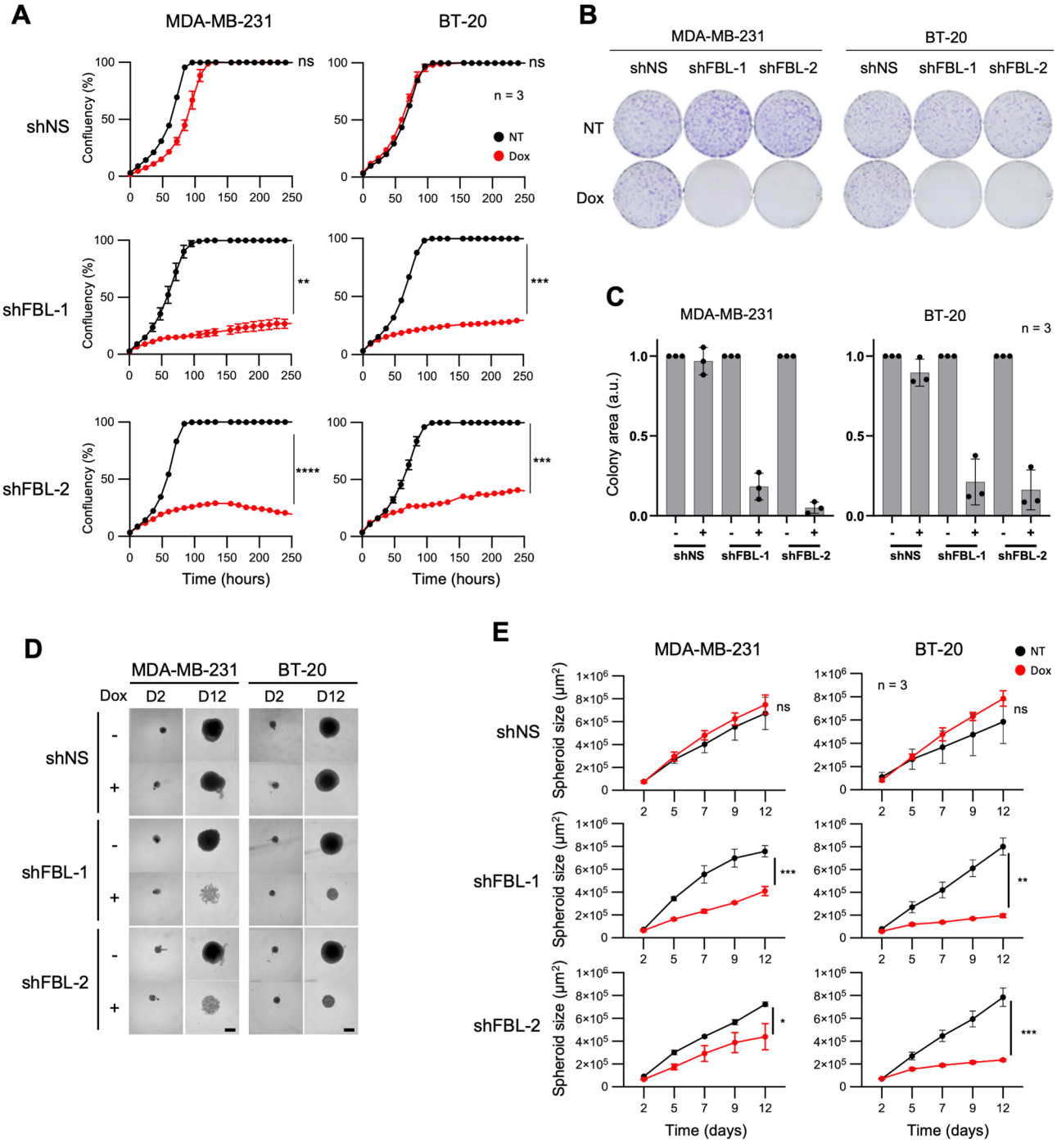


Fig. 6 Knock-down of FBL exerts an antitumoral activity on TNBC cells. **A,** Real time monitoring of the proliferation of MDA-MB-231 and BT-20 cell lines following induction of shRNA expression with doxycycline (Dox), compared to non-induced cells (NT). Data represent mean ± s.d. of three technical replicates. Student t-test. Data are representative of three biological replicates. **B-C,** Colony formation assay with MDA-MB-231 and BT-20 cell lines upon doxycycline induction of shRNA (shFBL-1, FBL-2, and shNS). Images in (**B**) are representative of three independent experiments at day 12. Quantification of colony surface area (**C**) from three biological replicates experiments. The surface area was normalised against the untreated condition for each doxycycline-treated condition. Data represent mean values ± s.d. and individual measurements (dots) **D-E,** Spheroid formation with MDA-MB-231 and BT-20 cells upon doxycycline induction (shFBL-1, FBL-2, and shNS). Phase contrast images were collected every 2 or 3 days, and representative images of spheroids at day 2 and day 12 are shown (**D**). Spheroid surface was quantified over time (**E**), with (Dox) or without (NT) doxycycline induction. Data represent the mean ± s.d. of three biological replicates

knock-down cells reached no more than 40% confluence, whereas non-treated cells achieved 100% confluence within 100 h (4 days) (Fig. 6A). To exclude any off-target effect of the shRNA approach, a rescue experiment was performed by expressing a tagged FBL protein, encoded by an shRNA resistant cDNA, in the shRNA-FBL cell lines (Figure S6). In these cell lines, the endogenous FBL became undetectable and was replaced by Flag-FBL at a similar level (Figure S6A). Rescuing FBL by Flag-FBL fully restored the growth capacity of both MDA-MB-231 and BT-20 cell lines, thus excluding an off-target effect (Figure S6B). Second, loss of FBL impacted also colony formation and growth (Fig. 6B), which decreased by 80% to 95% in FBL knock-down cells compared to control conditions (Fig. 6C). Third, we determined whether FBL knock-down also impaired the proliferation of cells grown in 3D as spheroids, by inducing shRNA expression with doxycycline for 12 days. Upon expression of either one of the FBL shRNAs, the spheroids were significantly smaller than non-treated control and shNS spheroids (Fig. 6D and E). After 12 days, shFBL-1 reduced the size of MDA-MB-231 spheroid by 1.8-fold, while shFBL-2 caused a 1.6-fold reduction. In BT-20 cells, shFBL-1 reduced spheroid size by fourfold, and shFBL-2 by 3.3-fold (Fig. 6E). Additionally, we noticed that shFBL-expressing spheroids exhibited an altered structure, characterized by a lower cell density and irregular edges, a phenotype that was more pronounced on MDA-MB-231 spheroids than on BT-20 spheroids (Fig. 6D). In conclusion, our data show that decreasing FBL expression inhibits cell growth of TNBC cells in vitro.

FBL knock-down induces cell cycle defects but no cell death in TNBC cells in vitro

We next characterized the mechanisms underlying the anti-tumoral effects of FBL knock-down. After 96 h of FBL knock-down, no evidence of cell death was observed using DRAQ7 staining (below 0.5%), while actinomycin D treatment led to 20 to 40% cell death, as reported above (Fig. 7A and Figure S3A). Our above results indicated that the caspase 3 and PARP cleavage are defective in both TNBC cell lines (Figure S3B). Consistently, FBL knock-down using shRNA or siRNA did not induce any significant difference in the expression or cleavage of caspase 3 and PARP proteins (Figure S7A and S7B). Thus, as observed with RNA Pol I inhibitors, ribosome inhibition by FBL knock-down did not trigger cell death in our TNBC cellular models.

In contrast, we observed that FBL knock-down impaired cell cycle progression, after either four days (D4) or seven days (D7) of shRNA induction (Fig. 7C and S7B). In both cell lines and for both FBL shRNAs, we observed an increase in G2/M phase and a strong decrease in S-phase. A more pronounced effect was observed in cells treated for seven days (Fig. 7B and Fiure S7C). Our results highlight that inhibiting rRNA maturation leads to cell cycle arrest in TNBC, an effect that appears to be more pronounced than the one triggeregd by CX-5461 and BMH-21 RNA Pol I inhibitors.

FBL knock-down induces tumor growth defects in TNBC xenografts

Finally, we assessed whether the in vitro anti-tumoral effect resulting from FBL knock-down could be replicated in an in vivo xenograft model. The MDA-MB-231 cells expressing shFBL-1, shFBL-2 and shNS were subcutaneously xenografted into athymic nude mice. Once tumors were established, shRNA expression was induced by providing the mice with 1 mg/mL doxycycline in their drinking water (Fig. 8A and Figure S8). In the MDA-MB-231 model, tumors with FBL knock-down exhibited a significantly reduced growth compared to both the vehicle control and shNS groups, starting 6 to 8 days post-induction (Fig. 8A). Tumor growth was negligible in the shFBL-1 model and strongly reduced in the shFBL-2 model. Immunohistochemistry confirmed a marked reduction in FBL expression only in the dox-treated shFBL xenograft, and neither in the shNS xenograft nor in the non-treated controls (Fig. 8B). Importantly, there was no significant weight loss observed in any of the mice throughout the experiment (Figure S8). Thus, FBL knock-down reduces growth of xenografted MDA-MB-231 cells. Consistent with the in vitro data, no cleaved caspase 3 was detected in xenografts tumors by IHC (Fig. 8B). Additionally, Ki67 and phospho-Histone H3 (Ser10) signals were strongly reduced upon FBL shRNA expression (Fig. 8B), corroborating the in vitro findings that FBL knock-down impairs cell cycle progression.

Together, these results demonstrate that inhibition of rRNA maturation through FBL depletion exerts anti-tumoral effects on TNBC xenografts in vivo by promoting cell cycle arrest.

Discussion

Given the poor response of TNBC patients to current standard-of-care treatments and their relapse, novel therapeutic strategies are urgently needed. The anti-cancer effects of ribosome biogenesis inhibition are well-supported by preclinical and clinical studies across various solid and haematological cancers. In this study, we demonstrate that ribosome biogenesis is an actionable vulnerability in TNBC, using two different strategies to inhibit ribosome production: suppression of rRNA synthesis and disruption of rRNA maturation.

Alterations in ribosome biogenesis have been reported in multiple cancer types, including TNBC, where the ribosome biogenesis machinery and RNA Pol I regulatory pathways are frequently dysregulated [20, 24, 28].

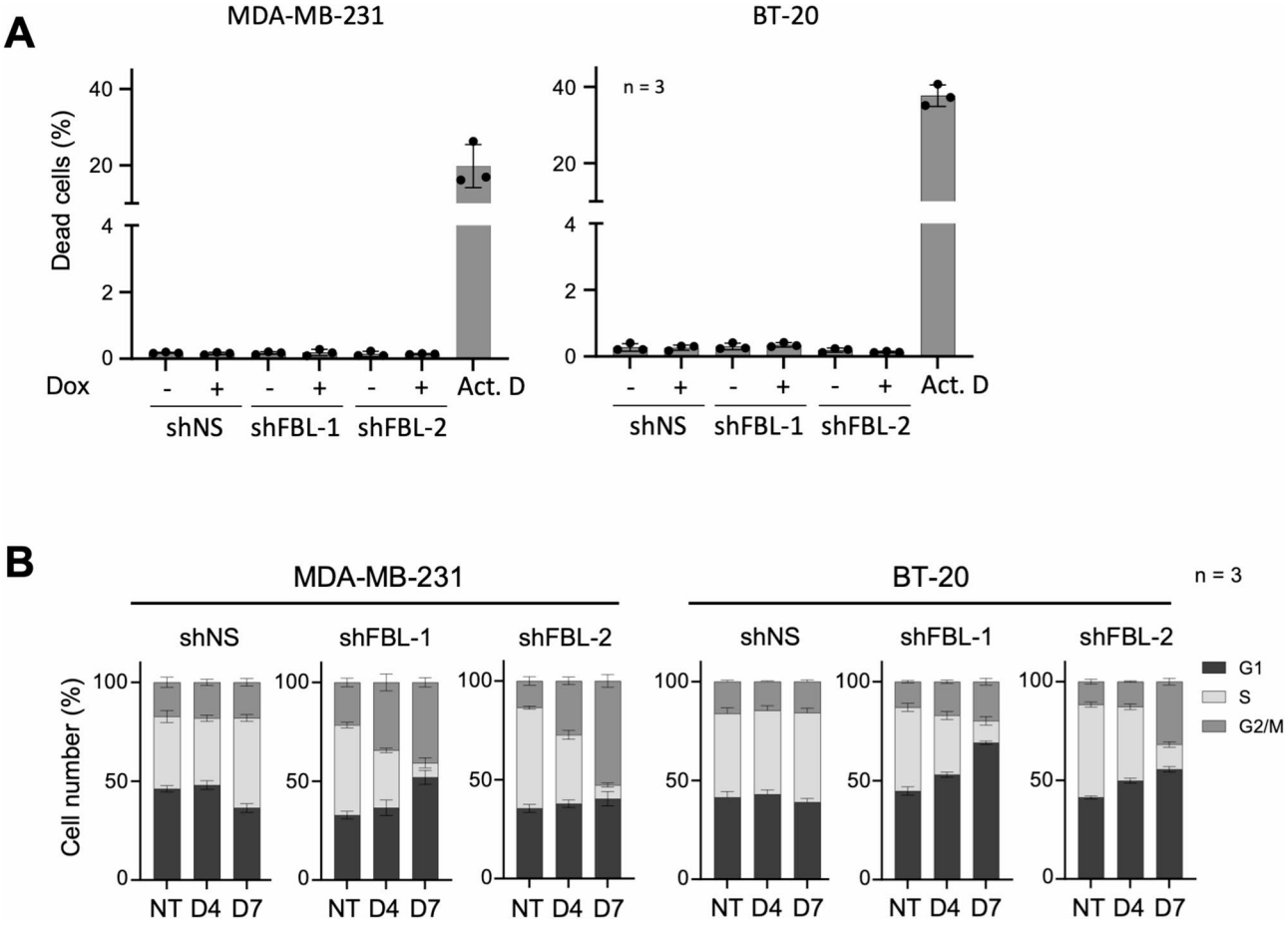


Fig. 7 Knock-down of FBL induces cell cycle defect but no cell death. **A,** Cell death analysis on MDA-MB-231 and BT-20 cells following 4 days of doxycycline induction (shFBL-1, FBL-2, and shNS) or 18 h treatment with actinomycin D, measured by DRAQ7 staining and fluorescence imaging. Data represent mean values ± s.d. of the percentage of dead cells from a technical triplicate, and are representative of two independent biological replicates. **B,** Proportion of cells in G1, S, and G2 phases of the cell cycle of MDA-MB-231 and BT-20 cells, following doxycycline-mediated expression of shRNA (shFBL-1, FBL-2, and shNS) for 4 or 7 days. Data are mean values ± s.d. of three technical replicates. Results are representative data of three biological replicates

Using transcriptomic data from The Cancer Genome Atlas (TCGA) and a ribosome biogenesis signature comprising 240 genes, we now provide evidence that ribosome biogenesis activity is more elevated in TNBC than in other breast cancer subtypes. Notably, this heightened ribosome biogenesis activity is summarized by a single key factor: the rRNA maturation factor FBL. Our findings reveal that FBL expression is markedly higher in TNBC than in other breast cancer subtypes, providing direct evidence of its link to this aggressive tumor type. TNBC thus represents an additional aggressive cancer subtype characterized by pronounced overactivation of ribosome biogenesis. The abnormal overactivation of ribosome biogenesis in TNBC provides one possible explanation for the sensitivity of TNBC cells to ribosome biogenesis inhibition that we observed in this study. Further studies will be required to extend our observations across additional cell line models that represent the full heterogeneity of the TNBC subtype.

Since the early 2010s, there has been a renewed interest in ribosome biogenesis as a therapeutic target with the discovery and exploitation of the new generation of RNA Pol I inhibitors CX-3543, CX-5461 and BMH-21 [7, 8, 29] (Bywater et al., 2012; Drygin et al., 2009; Peltonen et al., 2014). These compounds showed anti-tumoral activity on a wide range of pre-clinical models of haematological and solid tumors, including lymphoma, melanoma, osteosarcoma, and prostate and ovarian cancers [7, 8, 29–32]. Our data demonstrate that the RNA Pol I inhibitors CX-5461 and BMH-21 exhibit potent anti-tumoral activity in pre-clinical models of TNBC both in vitro and in vivo. In TNBC cells, these inhibitors effectively block pre-rRNA production, thereby disrupting ribosome biogenesis. However, the mechanism of action of both compounds relies on a direct interaction with DNA, particularly G4 quadruplexes and GC-rich sequences, which increases the risk of DNA-based off-target effects. While such off-target activity has herein been established

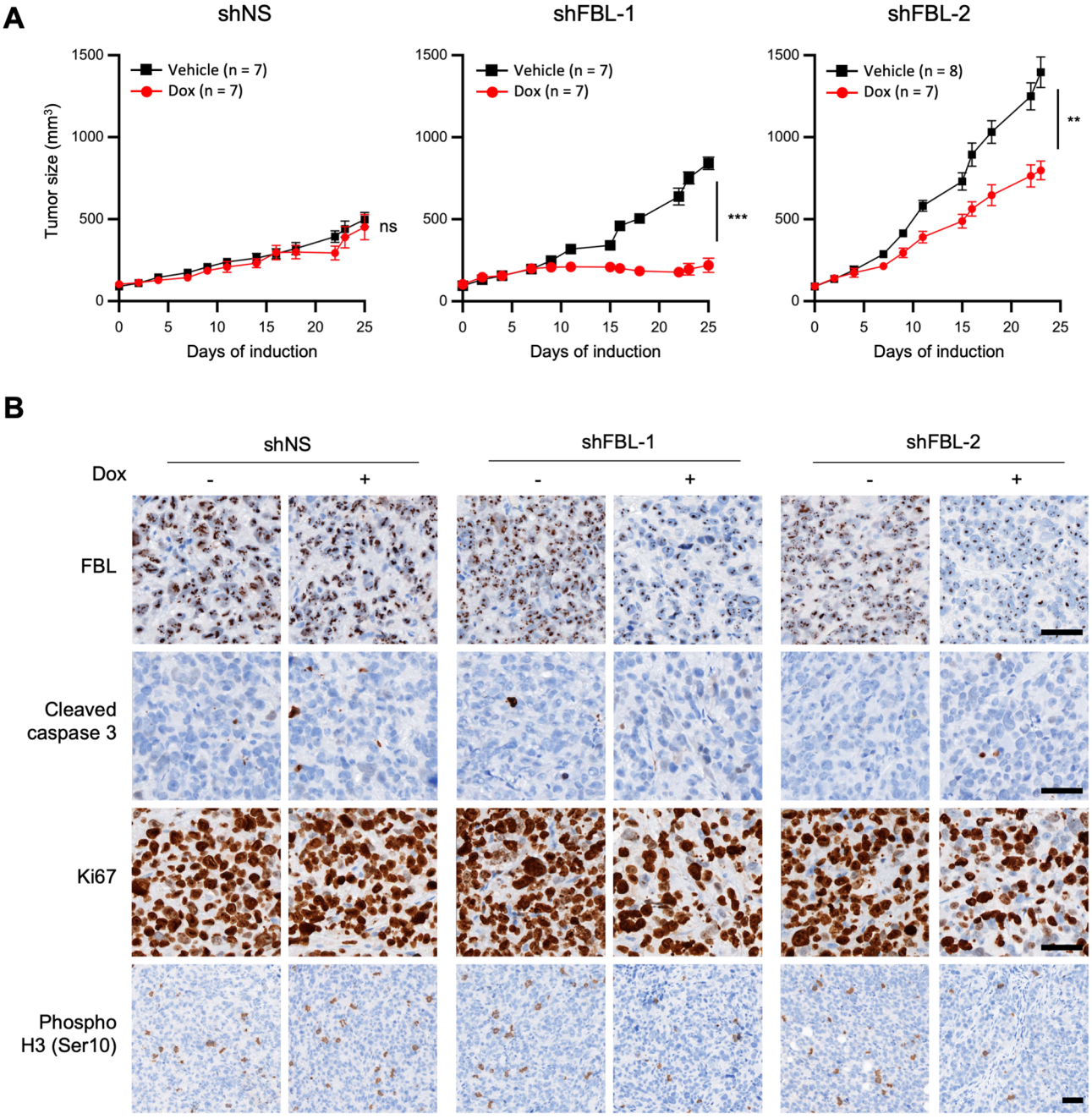


Fig. 8 FBL knock-down suppresses tumorigenicity in vivo in TNBC. **A,** Growth of tumor xenografts of MDA-MB-231 cell lines expressing either shFBL-1, shFBL-2, or shNS, upon doxycycline induction. Doxycycline was administered via drinking water for 25 days. Data are mean ± SEM. ** $p < 0.01$, *** $p < 0.001$ (Student t-test). **B,** Detection of FBL, cleaved caspase 3, Ki67 and phospho-histone H3 (Ser10) by IHC on tissue sections of MDA-MB-231 xenografted tumors from the experiment in (**A**). Images are representative of 5 xenografted tumors. Scale bar: 50 µm

for CX-5461 in TNBC and previously for other cancer types [9, 26], a detailed investigation into DNA-related off-target effects of BMH-21 remains to be conducted. In this study, we show that CX-5461, as actinomycin D, induced significant DNA damage and the accumulation of cells in S-phase, which indicate that cells undergo replication-stress, an observation supported by a previous study showing that CX-5461 acts as a Topoisomerase poison [26]. Consistently, CX-5461 displayed some toxicity in humans with frequent side effects (nausea, headaches), and significant phototoxicity [32, 33]. Collectively, these data highlight the need for safer and more specific strategies to target ribosome biogenesis. To this end, we explored the inhibition of rRNA maturation, and found that targeting FBL did not induce any detectable DNA damage. Collectively, these findings demonstrate the

potential of targeting the rRNA maturation process as a therapeutic strategy and identify FBL as a promising druggable target.

Ribosome maturation and assembly involve more than 200 factors, many of which are essential and represent additional potential targets, among which we, and others, identified the C/D box snoRNP [13–15]. In this study, we show that FBL represents an actionable target. We demonstrated that FBL knock-down prevents the cleavage of the 5'-ETS region in HeLa cells [16], and now in TNBC cellular models. These observations are consistent with the role of FBL in structuring U3 snoRNA, a snoRNA that plays an essential role in the folding and cleavage of the 5'-ETS region of the pre-rRNA [15]. It should be noted that FBL is a 2'-O-methyl transferase that modifies about 112 nucleotides in human rRNA [12, 19]. Future studies will be required to determine whether alterations in 2'-O-methylation contribute to the growth defects observed following FBL knockdown.

Ribosome biogenesis inhibition induces ribosomal stress, a cell response triggered by the accumulation of free ribosomal proteins, mainly uL18 (RPL5) and uL5 (RPL11), and ribosome biogenesis factors such as NPM1 [34], which activate the p53 pathway by trapping MDM2. Nonetheless, while p53 increases the sensitivity of cells to ribosomal stress, it is not required for the ribosomal stress-induced cell growth defect and cell death [35]. Accordingly, MDA-MB-231 and BT-20 cells displayed high sensitivity to RNA Pol I inhibitors, with IC_{50} in the low nanomolar range, and to FBL knock-down despite expressing a mutant p53 protein. This represents a key advantage for the development of the therapeutic inhibition of ribosome biogenesis, since the penetrance of *TP53* mutation is over 80% in TNBC [36]. In both TNBC cell lines used in this study, cell cycle arrest, but no apoptosis was observed after inhibition of ribosome biogenesis, whether through RNA Pol I inhibition or FBL knockdown. Such a phenotype is not specific to TNBC since apoptosis was not observed after ribosome biogenesis inhibition in several other models of cancer including melanoma (A375 cells), pancreatic cancer (MIA-PaCa cells), osteosarcoma (MNNG and U2OS cells) and prostate cancer (PC3, DU145 and LNCaP cells) [31, 35, 37]. However, our data indicate that the cell lines used in this study exhibit a defective apoptotic pathway, as they did not respond even to strong apoptosis inducers such as DNA damaging agent doxorubicin, including CX-5461, and kinase inhibitor staurosporine. Therefore, our observation may reflect the intrinsic apoptotic deficiency of these TNBC cell lines rather than the specific effect of ribosome biogenesis inhibition. The absence of apoptosis cannot be simply attributed to TP53 mutation. Indeed, there seems to be conflicting data since apoptosis was triggered upon CX-5461 treatment in TP53 mutated osteosarcoma cells lines [31], but was inhibited in lymphoma cells upon TP53 knock-down [38]. More globally, the contribution of p53 in the cell response to ribosome biogenesis inhibition remains to be defined [34]. Most importantly, we did not observe any cell death following RNA Pol I inhibition or FBL knock-down, indicating that ribosome biogenesis inhibition did not trigger alternative forms of cell death. Taken together, these results emphasize the central role of cell cycle defects, and further support the potential of targeting ribosome biogenesis as a therapeutic approach against apoptosis resistant tumors.

In summary, our findings highlight that targeting ribosome biogenesis represents a promising therapeutic strategy for TNBC, a breast cancer subtype in critical need of novel treatment approaches. Although the development of safer RNA Pol I inhibitors remains a potential avenue, our data strongly support the therapeutic potential of inhibiting ribosome maturation, specifically pre-rRNA cleavage, over rRNA synthesis. Furthermore, we highlight rRNA maturation factors, such as snoRNPs, as viable and druggable targets for anticancer therapy.

Material and methods

Cell culture and shRNA/siRNA transfection and treatments

MDA-MB-231 and BT-20 cells were cultured in DMEM-F12 medium (Life Technologies) supplemented with 1% GlutaMAX (Life Technologies), 10% foetal bovine serum (CliniSciences), and 1% penicillin–streptomycin (10,000 U/mL; Life Technologies). Cells were maintained at 37 °C in a humidified incubator with 5% CO_2.

MDA-MB-231 and BT-20 cell lines with inducible shRNA expression were generated via lentiviral infection. Lentiviral particles were produced using the vectors pTRIPZ-shRNA-NS and pTRIPZ-shRNA-351067 (FBL-1) and 351,068 (FBL-2), acquired from Open Biosystems (Dharmacon). The shRNA sequences used were as follows: shRNA-FBL-1: TGCATCTTTTTCACTTCGG, and shRNA-FBL-2: AGACCATCCGGACCAACGA, and a non-specific shRNA (shRNA-NS) as the control: GCG ATCTCGCTTGGGCGAGAGTAAGTA. Post-infection, cell populations were selected with 1 µg/mL puromycin for 14 days. shRNA expression was induced by treating the cells with 1 µg/mL doxycycline. Clonal populations were isolated through single-cell cloning and selected based on FBL expression following shRNA induction.

For the rescue experiment, we designed a shRNA resistant FBL cDNA, containing 12 silent mutations within the two sequences targeted by the shRNA-FBL-1 and FBL-2. The mutations are: C2204T, T2207C, T2210C, G2213A, T2216C, T2219C, C2220T, C2507G, A2510G, G2513C, A2516G, G2519A. The resulting cDNA, named FBL-shRes, was cloned in frame with the 3xflag and inserted in a piggybac vector by recombination (GenScript). The transgene was stably inserted by

transposition in the MDA-MB-231 and BT-20 cell lines expressing the shRNA-FBL-1, and cell lines were selected using 500 µg/mL hygromycin for 14 days.

For siRNA experiments, three siRNA duplexes were used for fibrillarin silencing as previously described [16]: "400":5'- UUU CCU CGA CAA AUG AAG AC –3', "882": 5'- AAA AUC ACA AAG UGU CCU CCA -3', "1090": 5'- UCU CUC GCA AUC CUG ACA G -3'. A non-targeting siRNA was used as a negative control (negative control siRNA duplex; Eurogentec SR-CL 000–005). Cells were transfected with these siRNAs using Interferin (Polyplus) following the manufacturer's instructions. Forty-eight- or seventy-two-hours post-transfection, cells were seeded for subsequent analyses.

CX-5461 was dissolved in 25 mM NaH_2PO_4 (pH 7.4), BMH-21 was dissolved in phospho-citrate buffer (pH 6), as previously described [7, 8]. Doxycycline was dissolved in water (Life Technologies). Actinomycin D was dissolved in ethanol at 5 mg/mL, Doxorubicin was dissolved in water at 2 mg/mL, Staurosporine and Etoposide were dissolved in water at 1 mM. All drugs were diluted at working concentration in cell culture medium.

Cell viability and IC_{50} measurement

IC_{50} values were determined using real-time growth monitoring with the Incucyte® S3 system (Sartorius®). For CX-5461 and BMH-21 treatments, cells were exposed to the compounds on day 0. For shRNA experiments, shRNA expression was induced with 1 µg/mL doxycycline 2 days prior to monitoring. Cells were seeded onto 96-well plates, and cell confluence was measured every 2 h. The IC_{50} of RNA polymerase I inhibitors at 96 h was calculated using Prism® software.

RNA extraction and RT-qPCR

RNA was extracted using the TRIzol®-chloroform method and quantified with a NanoDrop® 2000 spectrophotometer (Thermo Scientific®). Reverse transcription was performed on 200 ng of purified RNA using the PrimeScript™ RT kit (Takara®, RR037B) with random 6-mer primers. Quantitative PCR (qPCR) was conducted using the LightCycler® 480 SYBR Green I Master Mix (Roche®, 4,887,352,001) with specific primer pairs (see Supplementary Table S1) on the LightCycler® 96 instrument. Relative fold changes in gene expression were calculated using the 2^ – ΔΔCT method. The primer sequences were as follows: FBL-Fwd: 5'-CCT GGG GAA TCA GTT TAT GG3'; FBL-Rev: 5'-CCA GGC TCG GTA CTC AAT TTT-3'; GAPDH-Fwd: 5'-GCC CAA TAC GAC CAA ATC CAGC-3'; GAPGH-Rev: 5'-CAC ATC GCT CAG ACA C-3'.

Western blot

Ten to forty micrograms of whole-cell protein extract were separated on 12% or 4%-20% gradient SDS–polyacrylamide gels. Proteins were then transferred onto a 0.2 µm nitrocellulose membrane. The membrane was blocked with 5% non-fat milk in TBST (Tris-buffered saline with 0.1% Tween 20) for 1 h at room temperature. Primary antibodies (listed below) were incubated with the membrane for 1 h at room temperature or overnight at 4 °C in 5% milk-TBST. Proteins were detected by chemiluminescence using anti-rabbit or anti-mouse HRP-conjugated secondary antibodies (7074/7076, HRP-linked secondary antibodies, Cell Signaling Technology®) diluted 1:5000, and Clarity™ ECL substrate (Bio-Rad®). Alternatively, proteins were detected using fluorescent secondary antibodies (12,004,161/12005867, StarBright Blue 700, Bio-Rad®). Images were acquired using the ChemiDoc™ MP Imaging System (Bio-Rad®), and signal intensities were analysed using ImageLab™ software (Bio-Rad®).

Colony formation assay

Colony-forming assays were performed by seeding 1,000 cells per well in a 6-well plate. After 24 h, cells were treated with different concentrations of RNA polymerase I (Pol I) inhibitors. For shRNA-expressing cells, doxycycline was added at the time of plating. After 10 days, the colonies were fixed with 4% paraformaldehyde for 15 min at room temperature, stained with 1% crystal violet for 2 h at room temperature under gentle agitation, and washed with PBS. Colony counts were performed using ImageJ software with Guzman's plugin [39].

Spheroid formation assay

Five hundred cells were plated in 96-well ultra-low attachment (ULA) plates in 2.5% Matrigel medium. For wild-type cells, spheroids were treated with different concentrations of Pol I inhibitors (CX-5461, BMH-21, or Actinomycin D) 24 h post-plating. For shRNA-expressing cells, doxycycline induction was performed 2 days prior to plating. Spheroid growth was monitored using the Opera Phenix® High-Content Screening System (Revvity™). Spheroid size was measured using Signal Image Artist (SImA) software (Revvity™).

Immunofluorescence (IF)

Cells cultured on 96-well plates or coverslips were fixed with 4% paraformaldehyde for 5 min at room temperature and then permeabilized with 0.5% Triton X-100 for 5 min at room temperature. Cells were blocked with 3% FBS in PBS for 30 min. Primary antibodies (Supplementary table S5) were incubated with the cells for 1 h at room temperature, followed by incubation with fluorescence-labelled secondary antibodies for 30 min. Nuclei

were stained with Hoechst (0.5 µg/mL). Images were acquired using an Opera Phenix® High-Content Screening System (Revvity™).

Cell cycle analysis

Cells were cultured in 96-well plates and treated for 18 h with CX-5461, BMH-21, or actinomycin D, or for 3 and 7 days with doxycycline for shRNA induction. Cells were then incubated with 5-Ethynyl-2'-deoxyuridine (EdU, 1 mM) for 1 h at 37 °C with 5% CO_2 in a humidified incubator. Following incubation, cells were fixed with 4% paraformaldehyde for 5 min at room temperature and permeabilized with 0.5% Triton X-100 for 20 min at room temperature. Click detection was performed using a fluorescent-azide mix for 30 min, protected from light. Cells were then blocked with 3% FBS in PBS for 30 min and incubated with primary Phospho-Histone H3 (Serine 10) antibody (Merk® #06–570) for 1 h at room temperature. This was followed by incubation with fluorescence-labelled secondary antibodies for 30 min. Nuclei were stained with Hoechst (0.5 µg/mL). Cells were imaged using an Opera Phenix® automated microscope (Revvity™), and cell cycle phases were determined based on EdU signal (S-phase), Phospho-Histone H3 signal (M-phase), and Hoechst staining (G1 and G2/M phases) using SImA software (Revvity™).

Fluorescence In situ hybridization (FISH)

The FISH experiments were performed as described previously [40]. MDA-MB-231 and BT-20 cells were seeded on coverslips in 24-well plates. Cells were treated with CX-5461, BMH-21 (1 µM), or Actinomycin D (0.05 µg/mL) for 4 h. Cells were then fixed with 4% formaldehyde for 30 min. Cells were incubated with 2.5 ng of ETS-1 probe for 5 h in a humidified chamber at 37 °C. Images were acquired using a Zeiss Axio Imager widefield fluorescence microscope, a Zeiss LSM 980 confocal microscope, and an Opera Phenix® High-Content Screening System (Revvity™). The sequences of the probes were previously published [40]. ETS1 probe: AGACGAGAACGCCTGACACGCACGGCAC-AlexaFluor 555. 5'-ITS1 probe: CCTCGCCCTCCGGGCTCCGTTAATGATC-AlexaFluor 488.

Northern blot

RNA samples were analysed by northern blot as previously described [41]. Briefly, total RNAs were resolved by electrophoresis on 1.2% agarose, 6% formaldehyde, 0.02 M 3-(*N*-morpholino) propanesulfonic acid (MOPS) gels. Transfers were performed by capillarity on a nylon membrane (Nytran SuperCharge, Whatman) with 10X SSC (1.5 M sodium chloride, 0.15 M sodium citrate, pH 7.0). Membranes were incubated overnight at 42 °C with hybridization buffer (ULTRAhyb™-Oligo, Invitrogen) containing ITS1 or ITS2 DNA probes. Membranes were washed four times with 0.1X SSC and 0.1% SDS before signal exposure on ChemiDoc MP (Bio-Rad). Quantification was performed using Image Lab software (Bio-Rad) and relative 47S pre-rRNA levels were determined by normalisation against intermediate ARNr levels. The probe sequences were as follows:

ITS15′- CCGCGGGCCTCGCCCTCCGGGCTCCGTTAATGATCCTTCC-Dylight 800.

ITS25′- CTGCGAGGGAACCCCCAGCCGCGCA-Dylight 800.

Cell death detection with DRAQ7

Two thousand cells (MDA-MB-231 and BT-20) per condition were cultured in 96-well plates. Cells were treated with RNA Pol I inhibitors one day after plating for 3 days, or at the time of plating for shRNA-expressing cells for 4 days. Subsequently, cells were stained with DRAQ7 (1:1000, 424,001 BioLegend® Inc.) and nuclei were counterstained with Hoechst (0.5 µg/mL) for 3 h. The cells were then imaged using an Opera Phenix® High-Content Screening System (Revvity™), and DRAQ7(positive cells were quantified using SImA software (Revvity™).

Caspase 3/7 incucyte® assay

Two thousand cells (MDA-MB-231 and BT-20) per condition were plated in 96-well plates. Cells were treated 24 h post-plating with Pol I inhibitors (CX-5461, BMH-21, actinomycin D), or directly with doxycycline for shRNA-expressing cells, including a 2-day pre-treatment. Incucyte® Caspase 3/7 Green Dye was added to the medium as recommended by the manufacturer (Thermo Fisher Scientific®). Cells were monitored in real-time using the Incucyte® S3 system (Sartorius®) for one week, with images captured every 2 h. Apoptotic cells were quantified using Incucyte® software.

Xenograft models

Five-week-old female athymic nude mice were obtained from JANVIER® and maintained under specific pathogen-free conditions. The animal protocol described below was reviewed and approved by the Animal Ethical and Welfare Committee (protocol number: 2021101416573294). A total of 2×10^6 MDA-MB-231 cells or 3×10^6 BT-20 cells (normal [WT or shNC] or FBL-depleted [shFBL-1, -2]) were inoculated subcutaneously into the dorsal flank of the nude mice in PBS. Treatment with CX-5461, BMH-21, doxycycline, or vehicle was initiated once the tumors reached a similar size (approximately 100 mm^3). Mice were randomly assigned to control and treatment groups. CX-5461 (50 mg/kg) dissolved in 25 mM NaH_2PO_4 (pH 7.4) was administered via oral gavage three times per week. BMH-21 (50 mg/kg) dissolved in phospho-citrate (pH 6.0) was administered via intraperitoneal injection

five times per week. Doxycycline (2 mg/mL) dissolved in water with 3% sucrose was provided in drinking water continuously. Mouse weight was monitored weekly, and tumor size was measured three times per week using callipers. Animal experimental procedures and immunohistochemical staining were carried out by the Small Animal Platform (P-PAC) and the Pathology-Research Platform of the Cancer Research Center of Lyon (CRCL).

Trypsin digestion and mass spectrometry analysis

For mass spectrometry analysis, 5 independent whole cell extracts were prepared from MDA-MB-231 cells untreated or treated for 18 h with CX-5461 at 700 nM, BMH-21 at 1000 nM, or Actinomycin D at 0.05 µg/mL, using a lysis buffer containing 62.5 mM Tris–HCl, 1% SDS and 1 mM DTT. Protein concentration was measured using TCA precipitation assay. Between 40 µg and 100 µg of proteins were subjected to a disulfide bridge reduction for 10 min at 95 °C under agitation followed by an alkylation of cysteine residues in 60 mM iodoacetamide for 30 min in the dark at room temperature. Each reduced/alkylated protein sample was then digested using the S-Trap™ micro spin column protocol [https://doi.org/10.1021/acs.jproteome.8b00505]. Briefly, equiva lent volumes of 10% SDS were added to each sample in order to reach a final SDS concentration of 5%. Undissolved matter was removed by centrifugation for 8 min at 13,000 × g. Aqueous phosphoric acid (12%) was added at a ratio of 1:10 to the protein sample for a final concentration of ~ 1.2% phosphoric acid, followed by seven volumes of S-Trap binding buffer (90% methanol, 100 mM TEAB, pH 7.1). After gentle mixing, the protein solution was loaded into an S-Trap filter several times, each separated by a 4000 × g centrifugation step, until all the SDS lysate/S-Trap buffer had passed through the column. Afterwards, the captured proteins were washed six times with 150 µL S-Trap binding buffer. Digestion was performed overnight at 37 °C by the addition of 20 µL of trypsin (Sequencing Grade Modified Trypsin, Promega) at 37.5 ng/µL in 50 mM ammonium bicarbonate. The digested peptides were eluted by the addition of 35 µL of 50 mM ammonium bicarbonate and 1 min centrifugation at 4000 × g, followed by 35 µL of 0.2% formic acid and 4000 × g centrifugation (1 min) and finally 40 µL of 50% aqueous acetonitrile containing 0.2% formic acid and a last 1 min centrifugation step at 4000 × g. Before drying down the pooled eluates under speed vacuum, the peptide amount was measured using the Pierce Quantitative Fluorometric Peptide assay (Thermo Fisher Scientific®).

Based on the fluorometric peptide assay, samples were resuspended in 2% acetonitrile (ACN), 0.2% formic acid (FA) at a concentration of 250 ng/µL and sonicated for 10 min before analysis by online nanoLC-MS/MS using an UltiMate® 3000 RSLCnano LC system (Thermo Scientific, Dionex) coupled to an Orbitrap Exploris 480 mass spectrometer using FAIMS Pro Duo interface (Thermo Fisher Scientific, Bremen, Germany). One microliter of each sample was directly loaded onto the analytical C18 nanocolumn (Acclaim PepMap RSLC C18 75 µm ID × 50 cm, 2 µm, 100 Å, Thermo Fisher Scientific) heated at 45 °C and equilibrated in 97.5% solvent A (0.2% formic acid) and 2.5% solvent B (80% ACN, 0.2% formic acid) during 16 min at a flow rate of 300 nL/min. Peptides were eluted using a gradient of 2.5% to 25% of solvent B for 102 min, then 25% to 40% of solvent B for 20 min at a flow rate of 300 nL/min (165 min running time and 122 min total gradient time). The Orbitrap Exploris 480 was operated in FAIMS mode (Standard Resolution, gas flow of 3.9 L/min and two compensation voltages used: – 45 V and – 60 V) and in data-dependent acquisition mode using a top-speed approach (cycle times of 0.8 s and 0.7 s, respectively for each CV) with the Xcalibur software. For both CV experiments, the following parameters were used: Survey scans MS were acquired in the Orbitrap on the 375 – 1200 m/z range, with the resolution set to a value of 60 000, a « Normalized AGC target» at 300% and a « Maximum injection time» at 60 ms for -45 V and 50 ms for -60 V. The most intense multiply charged ions (2 + to 6 +) above a threshold ion count of 5 × 103 were selected, for fragmentation by higher energy collisional dissociation with an isolation window of 1.6 m/z and a normalized collision energy of 30%. The resulting fragments were analysed in the Orbitrap at 15,000 resolution, a « Normalized AGC target» at 100% and a « Maximum injection time» set to Auto. Dynamic exclusion was used within 45 s with a 10 ppm tolerance, to prevent repetitive selection of the same peptide. For internal calibration the 445.120025 ion was used as lock mass in the first MS Experiment for the first five minutes using a CV at -30 V with a 120,000 resolution.

MS-based protein identification and label-free quantitative proteomics analysis

All raw MS files were processed with MaxQuant software (v 2.5.1.0) for database search with the Andromeda search engine and for quantitative analysis. Spectra were searched against the human proteins in the Uniprot Reference Proteome database (database release version of April 2023), containing 81,791 sequences (downloaded from http://www.uniprot.org), and the set of common contaminants provided by MaxQuant. Carbamidomethylation of cysteines was set as a fixed modification, whereas oxidation of methionine and protein N-terminal acetylation were set as variable modifications. Specificity of trypsin digestion was set for cleavage after K or R, and two missed trypsin cleavage sites were allowed. The precursor mass tolerance was set to 20 ppm for the first search and 4.5 ppm for the main Andromeda database

search. The mass tolerance in tandem MS mode was set to 20 ppm. The minimum peptide length was set to seven amino acids, and the minimum number of unique or razor peptides was set to one for validation. Andromeda results were validated by the target decoy approach using a reverse database, with a false discovery rate set at 1% at both PSM (peptide sequence match) and protein level. For label-free relative quantification of the samples, the match between runs option of MaxQuant was enabled with a match time window of 0.7 min, to allow cross-assignment of MS features detected in the different runs, after alignment of the runs with a time window of 20 min. Proteins were quantified by the MaxLFQ algorithm integrated in the MaxQuant software. A minimum ratio count of two unique or razor peptides was required for quantification.

Statistical analysis of the proteomic data was performed in the Perseus software (version 1.6.15.0) after loading the "proteinGroups.txt" files from MaxQuant. Reverse database hits were removed as well as proteins identified as contaminants. LFQ intensities were log2 transformed and replicate samples were grouped. Proteins with less than three valid values in at least one group were removed and missing values were imputed from a normal distribution around the detection. For each pairwise comparison, an unpaired two-tailed Student t test was performed, and proteins were considered differentially abundant when their absolute log2-transformed fold change (FC) was higher than 1 and their p-value lower than 0.05. Volcano plots were drawn to visualize significant protein abundance variations between the compared conditions. These represent $-\log_{10}$ (p-value) according to the $\log_2$ ratio. The complete list of the identified and quantified proteins and analysed according to this statistical procedure is described in Table S6.

TCGA breast cancer cohorts and statistical analyses

Gene expression BRCA dataset were uploaded from the TCGA database [25]. Gene expression was given as "log2(norm_count + 1)". After data upload and transformation, a BRCA tumor dataset was built by conserving only tumoral tissues collected at diagnosis from women without any neoadjuvant treatment at primary site and for which status of either PAM50 or oestrogen, progesterone and HER2 receptors was available. The gene signatures were derived by calculating the median expression of genes involved in each signature per tumor, the RiBi signature being composed of 240 genes (Supplementary Table 1 "signature") and the snoRNP signature of 4 genes. For each gene signature, mean comparison was performed between four breast cancer subtypes. Two classifications were used: PAM50 as given by the TCGA database; and intrinsic breast cancer status determined using the oestrogen, progesterone and HER2 receptors' IHC data given by the TCGA database (Supplementary Tables S2-S3). Prior to mean comparison, application conditions of statistical tests were performed (normality: Shapiro–Wilk test; homogeneity of variances: Levene test). Comparison between all breast cancer subtypes was performed using ANOVA. If significant, a two-by-two comparison was assessed using either parametric Student t-tests or nonparametric Mann–Whitney tests depending on results of the control of the application conditions. P-values of two-by-two comparison were then adjusted to multiple testing using False Discovery Rate method. Statistical significance was based on a $p < 0.05$ where the H0 hypothesis is rejected. Violin plots were used to visualize the distribution per breast cancer subtype. Statistical analyses and visualisations were performed using R Studio (version 2024.04.1 + 748).

Statistical analysis and graphical representations

Statistical analyses (ANOVA, Student t-test) and graphical representations were performed with GraphPad PRISM 10.

Supplementary Information

The online version contains supplementary material available at https://doi.org/10.1186/s13058-025-02163-x.

Supplementary Material 1

Supplementary Material 2

Supplementary Material 3

Supplementary Material 4

Supplementary Material 5

Acknowledgements

We thank the core facilities of the Cancer Research Center of Lyon for technical help: in particular Mélina GAUTIER (PIC Cellular Imaging Platform of CRCL), Isabelle GODDARD (P-PAC animal core facility), Nicolas GADOT (PAR research pathology platform) and Maxime GARCIA (Center for Drug Discovery and Development, Centre Léon Bérard). We thank Brigitte Manship for editing the manuscript. We are grateful to Thierry DUBOIS (Institut Curie, Paris, France) for providing the TNBC cell lines.

Author contributions

CJ, PLM, AG, CI, FB, M-AM, MM, MCD, CF, JM, LB and SD performed experiment and analysed data. JR, FNVL, TF, VM and FC analysed data. CV contributed to methodology. FC, CJ, SG and VM conceived the study. FC, JJD and VM secured funding. JJD and VM reviewed the manuscript. CJ, PLM and FC wrote and reviewed the manuscript.

Funding

The study was supported by grants from: La ligue régionale Contre le Cancer région AURA to FC, ANR (Actimeth, 19-CE12-0004; LabEx DEVweCAN, ANR-10-LABX-0061; Institut Convergence ANR-17-CONV-0002), European network COST Translacore (COST Action CA21154). This work was supported in part by the French Ministry of Research with the Investissement d'Avenir Infrastructures Nationales en Biologie et Santé program (ProFi, Proteomics French Infrastructure project; ANR-10-INBS-08). C.J. and J.R. received a PhD fellowship from the Ligue Nationale Contre le Cancer. P.L.M. received a PhD fellowship from the French Ministry for higher education and research. FNVL received a PhD fellowship from Ligue Nationale Contre le Cancer and

Fondation pour la Recherche Médicale. F.C. is a CNRS research fellow. V.M., S.D. and J.-J.D. are Inserm research fellows.

Availability of data and material

The mass spectrometry proteomics data have been deposited to the ProteomeXchange Consortium via the PRIDE [42] partner repository with the dataset identifier PXD060027. All other raw data are available upon request from the corresponding author. Biological material is available upon reasonable demand.

Declarations

Ethics approval and consent to participate

The animal protocol described in this study was reviewed and approved by the Animal Ethical and Welfare Committee (protocol number: 2021101416573294).

Consent for publication

Not applicable.

Competing interest

Authors declare no competing interest.

Author details

[1]Ribosome, Translation and Cancer Team, LabEx DEVweCAN, Institut Convergence Plascan, LyriCAN+, Centre de Recherche en Cancérologie de Lyon (CRCL), INSERM U1052, CNRS UMR 5286, Centre Léon Bérard, Université de Lyon, Université Claude Bernard Lyon 1, 69008 Lyon, France
[2]Institut de Pharmacologie Et de Biologie Structurale (IPBS), Université de Toulouse, CNRS, Toulouse, France
[3]Infrastructure Nationale de Protéomique, ProFI, UAR, 2048 Toulouse, France
[4]Cellular Imaging Platform, Centre de Recherche en Cancérologie de Lyon (CRCL), INSERM U1052, CNRS UMR 5286, Centre Léon Bérard, Université de Lyon, Université Claude Bernard Lyon 1, 69008 Lyon, France
[5]Center for Drug Discovery and Development, Synergie Lyon Cancer Foundation, Lyon Cancer Research Center, Centre Léon Bérard, 69373 Lyon Cedex 08, France

Received: 22 April 2025 / Accepted: 27 October 2025
Published online: 13 November 2025

References

1. Bianchini G, De Angelis C, Licata L, Gianni L. Treatment landscape of triple-negative breast cancer — expanded options, evolving needs. *Nature Reviews Clinical Oncology 2021* 2021; **19**: 91–113.
2. Cardoso F, Paluch-Shimon S, Senkus E, Curigliano G, Aapro MS, André F, et al. 5th ESO-ESMO international consensus guidelines for advanced breast cancer (ABC 5). Ann Oncol. 2020;31:1623–49.
3. Li Y, Zhang H, Merkher Y, Chen L, Liu N, Leonov S *et al.* Recent advances in therapeutic strategies for triple-negative breast cancer. *J Hematol & Oncol* 2022; **15**: 1–30.
4. Drygin D, Rice WG, Grummt I. The RNA polymerase I transcription machinery: an emerging target for the treatment of cancer. Annu Rev Pharmacol Toxicol. 2010;50:131–56.
5. Pelletier J, Thomas G, Volarevic S, Volarevi S. Ribosome biogenesis in cancer: new players and therapeutic avenues. Nat Rev Cancer. 2017;18:51–63.
6. Ferreira R, Schneekloth JS, Panov KI, Hannan KM, Hannan RD. Targeting the RNA polymerase I transcription for cancer therapy comes of age. Cells. 2020;9:266.
7. Bywater MJ, Poortinga G, Sanij E, Hein N, Peck A, Cullinane C, et al. Inhibition of RNA polymerase I as a therapeutic strategy to promote cancer-specific activation of p53. Cancer Cell. 2012;22:51–65.
8. Peltonen K, Colis L, Liu H, Trivedi R, Moubarek MS, Moore HM, et al. A targeting modality for destruction of RNA polymerase I that possesses anticancer activity. Cancer Cell. 2014;25:77–90.
9. Xu H, Di Antonio M, McKinney S, Mathew V, Ho B, O'Neil NJ *et al.* CX-5461 is a DNA G-quadruplex stabilizer with selective lethality in BRCA1/2 deficient tumours. *Nature Communications* 2017; **8**: 1–18.
10. Devlin JR, Hannan KM, Hein N, Cullinane C, Kusnadi E, Ng PY, et al. Combination therapy targeting ribosome biogenesis and mRNA translation synergistically extends survival in MYC-driven lymphoma. Cancer Discov. 2016;6:59–70.
11. Hald ØH, Olsen L, Gallo-Oller G, Elfman LHM, Løkke C, Kogner P, et al. Inhibitors of ribosome biogenesis repress the growth of MYCN-amplified neuroblastoma. Oncogene. 2019;38:2800–13.
12. Paraqindes H, Mourksi N-E-H, Ballesta S, Hedjam J, Bourdelais F, Fenouil T, et al. Isocitrate dehydrogenase wt and IDHmut adult-type diffuse gliomas display distinct alterations in ribosome biogenesis and 2'O-methylation of ribosomal RNA. Neuro Oncol. 2023. https://doi.org/10.1093/NEUONC/NOAD140.
13. Catez F, Dalla N, Marcel V, Zorbas C, Lafontaine DLJ, Diaz J. Ribosome biogenesis: an emerging druggable pathway for cancer therapeutics. Biochem Pharmacol. 2019;159:74–81.
14. Tafforeau L, Zorbas C, Langhendries JL, Mullineux ST, Stamatopoulou V, Mullier R, et al. The complexity of human ribosome biogenesis revealed by systematic nucleolar screening of pre-rRNA processing factors. Mol Cell. 2013;51:539–51.
15. Langhendries J-L, Nicolas E, Doumont G, Goldman S, Lafontaine DLJ, Langhendries J-L, et al. The human box C/D snoRNAs U3 and U8 are required for pre-rRNA processing and tumorigenesis. Oncotarget. 2016;5:3–8.
16. Erales J, Marchand V, Panthu B, Gillot S, Belin S, Ghayad SE, et al. Evidence for rRNA 2'-O-methylation plasticity: control of intrinsic translational capabilities of human ribosomes. Proc Natl Acad Sci U S A. 2017;114:12934–9.
17. Marcel V, Ghayad SE, Belin S, Therizols G, Morel AP, Solano-Gonzàlez E, et al. P53 acts as a safeguard of translational control by regulating fibrillarin and rRNA methylation in cancer. Cancer Cell. 2013;24:318–30.
18. Rodriguez-Corona U, Sobol M, Rodriguez-Zapata LC, Hozak P, Castano E. Fibrillarin from Archaea to human. Biol Cell. 2015;107:159–74.
19. Lo Monaco P, Marcel V, Diaz J-JJ, Catez F, Monaco P, Marcel V *et al.* 2'-O-methylation of ribosomal RNA: Towards an epitranscriptomic control of translation? *Biomolecules* 2018; **8**: 106.
20. Nguyen Van Long F, Lardy-Cleaud A, Carène D, Rossoni C, Catez F, Rollet P *et al.* Low level of Fibrillarin, a ribosome biogenesis factor, is a new independent marker of poor outcome in breast cancer. *BMC Cancer* 2022; **22**: 1–12.
21. Zhou F, Liu Y, Rohde C, Pauli C, Gerloff D, Köhn M, et al. AML1-ETO requires enhanced C/D box snoRNA/RNP formation to induce self-renewal and leukaemia. Nat Cell Biol. 2017;19:844–55.
22. Koh CM, Gurel B, Sutcliffe S, Aryee MJ, Schultz D, Iwata T, et al. Alterations in nucleolar structure and gene expression programs in prostatic neoplasia are driven by the MYC oncogene. Am J Pathol. 2011;178:1824–34.
23. Luo W, Lin S, Huang Y, Zhu K, Zhang F, Lin J, et al. Bioinformatic analysis and in vitro and in vivo experiments reveal that fibrillarin participates in the promotion of lung metastasis in hepatocellular carcinoma. Bioengineering. 2022. https://doi.org/10.3390/bioengineering9080396.
24. Su H, Xu T, Ganapathy S, Shadfan M, Long M, Huang TH, et al. Elevated snoRNA biogenesis is essential in breast cancer. Oncogene. 2014;33:1348–58.
25. Ciriello G, Gatza ML, Beck AH, Wilkerson MD, Rhie SK, Pastore A, et al. Comprehensive molecular portraits of invasive lobular breast cancer. Cell. 2015;163:506–19.
26. Bruno PM, Lu M, Dennis KA, Inam H, Moore CJ, Sheehe J, et al. The primary mechanism of cytotoxicity of the chemotherapeutic agent CX-5461 is topoisomerase II poisoning. Proc Natl Acad Sci U S A. 2020;117:4053–60.
27. Henras AK, Plisson-Chastang C, O'Donohue MF, Chakraborty A, Gleizes PE. An overview of pre-ribosomal RNA processing in eukaryotes. Wiley Interdiscip Rev RNA. 2015;6:225–42.
28. Ban Y, Zou Y, Lee SB, B.Bednarczyk R, Sheng J, Cao Y *et al.* Targeting Ribosome Biogenesis as a Novel Therapeutic Approach to Overcome EMT-related Chemoresistance in Breast Cancer. 2023. https://doi.org/10.7554/eLife.89486.1.
29. Drygin D, Siddiqui-Jain A, O'Brien S, Schwaebe M, Lin A, Bliesath J, et al. Anticancer activity of CX-3543: a direct inhibitor of rRNA biogenesis. Cancer Res. 2009;69:7653–61.
30. Fu X, Xu L, Qi L, Tian H, Yi D, Yu Y, et al. BMH-21 inhibits viability and induces apoptosis by p53-dependent nucleolar stress responses in SKOV3 ovarian cancer cells. Oncol Rep. 2017;38:859–65.
31. Li L, Li Y, Zhao J, Fan S, Wang L, Li X. CX-5461 induces autophagy and inhibits tumor growth via mammalian target of rapamycin-related signaling pathways in osteosarcoma. Onco Targets Ther. 2016;9:5985–97.

32. Khot A, Brajanovski N, Cameron DP, Hein N, Maclachlan KH, Sanij E, et al. First-in-human RNA polymerase I transcription inhibitor CX-5461 in patients with advanced hematologic cancers: Results of a phase I dose-escalation study. Cancer Discov. 2019;9:1036–49.
33. Hilton J, Gelmon K, Bedard PL, Tu D, Xu H, Tinker A V. *et al.* Results of the phase I CCTG IND.231 trial of CX-5461 in patients with advanced solid tumors enriched for DNA-repair deficiencies. *Nature Communications* 2022; **13**: 1–12.
34. Russo A, Russo G. Ribosomal proteins control or bypass p53 during nucleolar stress. Int J Mol Sci. 2017;18:1–16.
35. Drygin D, Lin A, Bliesath J, Ho CB, O'Brien SE, Proffitt C, et al. Targeting RNA polymerase I with an oral small molecule CX-5461 inhibits ribosomal RNA synthesis and solid tumor growth. Cancer Res. 2011;71:1418–30.
36. Koboldt DC, Fulton RS, McLellan MD, Schmidt H, Kalicki-Veizer J, McMichael JF, et al. Comprehensive molecular portraits of human breast tumours. Nature. 2012;490:61–70.
37. Rebello RJ, Kusnadi E, Cameron DP, Pearson HB, Lesmana A, Devlin JR, et al. The dual inhibition of RNA pol i transcription and PIM kinase as a new therapeutic approach to treat advanced prostate cancer. Clin Cancer Res. 2016;22:5539–52.
38. Domostegui A, Peddigari S, Mercer CA, Iannizzotto F, Rodriguez ML, Garcia-Cajide M, et al. Impaired ribosome biogenesis checkpoint activation induces p53-dependent MCL-1 degradation and MYC-driven lymphoma death. Blood. 2021;137:3351–64.
39. Guzmán C, Bagga M, Kaur A, Westermarck J, Abankwa D. Colonyarea: an ImageJ plugin to automatically quantify colony formation in clonogenic assays. PLoS ONE. 2014. https://doi.org/10.1371/journal.pone.0092444.
40. Therizols G, Bash-Imam Z, Panthu B, Machon C, Vincent A, Ripoll J, et al. Alteration of ribosome function upon 5-fluorouracil treatment favors cancer cell drug-tolerance. Nat Commun. 2022;13:173.
41. Durand S, Bruelle M, Bourdelais F, Bennychen B, Blin-Gonthier J, Isaac C, et al. RSL24D1 sustains steady-state ribosome biogenesis and pluripotency translational programs in embryonic stem cells. Nat Commun. 2023. https://doi.org/10.1038/S41467-023-36037-7.
42. Perez-Riverol Y, Bandla C, Kundu DJ, Kamatchinathan S, Bai J, Hewapathirana S, et al. The PRIDE database at 20 years: 2025 update. Nucleic Acids Res. 2025;53:D543–53.

Publisher's Note

Springer Nature remains neutral with regard to jurisdictional claims in published maps and institutional affiliations.